1. INTRODUCTION

Current design methods focus on crack growth curves which are material properties for given materials and environments. Structures subject to crack growth spend 90–95% of their lifetime in nucleation of very tiny flaws into measurable crack sizes. Due to the large variation in initial flaw sizes and the mathematics of flaw growth, the fatigue lifetimes, even of high-quality structures, can vary by a factor of as much as 10 to 20 even in a small fleet. This large variation in fatigue lifetimes leads to conservative statistics, which often prompts the premature retirement or overhaul of vehicles or other structures, since they focus on the weakest members of the fleet, while the remainder of the fleet is sound.

In the two past years, Oak Ridge National Laboratory (ORNL) has developed a new Griffith energy-based technique that can provide useful warning of the impending failure of a structure due to end-of-life crack propagation. This technique has been demonstrated by test and analysis in fiberglass composite, aircraft aluminum, and construction steel under pristine and corroded conditions, and for Mode I and Mode III fatigue, as well as Mode I low-temperature creep and stress corrosion.

During the 1930s, A. A. Griffith introduced the technique of considering crack growth in solids as a process of energy exchange in which external energy in introduced and stored as internal strain energy. During the process of crack growth, which is an energy consuming process, the internal strain energy and any additional externally introduced energy from loading is transformed into new crack surface area. When the rate of change of internal strain energy per unit crack length increase equals the rate of consumption of surface energy due to additional crack surface creation, a crack will begin to extend. This critical strain energy release rate, called G_{Ic}, then becomes a criterion for the onset of initial crack extension. The subscript, I, indicates Mode I crack growth, although the technique is also valid for the other two modes of crack growth, Modes II (in-plane shear) and Mode III (out-of-plane shear).

During the 1970s, J. R. Rice extended this technique to elastic-plastic materials through the introduction of a nonlinear-elastic version of this same criterion, J_{Ic}. The method applies Green's theorem to nonlinearly elastic loaded structures to express the sum of changes in internal strain energy plus changes in externally supplied energy due to crack growth. When the sum of these changes equals the surface energy of the material, a crack will begin to extend.

Since the 1970s, the brittle fracture and fatigue crack growth characteristics of materials have been measured as material properties, subject to certain environmental conditions. However, a considerable statistical variation still occurs in these crack growth rates, and the method of predicting the reaction of structures according to the particular material and environment has been very difficult to manage analytically. Loading amplitude and frequency, gaseous and liquid environment, temperature, loading mode (tension, flexure, or shear), and crack growth mode (Mode I, II, or III) all potentially may vary frequently and independently. This will introduce variables into the prediction of structural behavior that makes structural safety management uncertain, requiring large safety factors leading to underutilization of structural capacity.

During the last 20 years, Griffith energy-based criteria have also been used for other crack-growth-based failure mechanisms, such as the onset of crack growth in creep (or sustained loading of cracks) and stress corrosion cracking (K_{Iscc}, J_{Iscc}, sustained loading of cracks in aggressive environments).

Current design methods for fatigue focus on crack growth rate curves, which are material properties for given materials and environments. Structures subject to crack growth spend 80–90% of their lifetime in nucleation of very tiny flaws into measurable crack sizes. Due to the large variation in initial flaw sizes and the mathematics of flaw growth, the structure lifetimes of high-quality structures can vary by a factor of as much as 10 to 20 even in a small fleet. This large variation in structure lifetimes leads to conservative statistics, which often prompts the premature retirement or overhaul of vehicles or other structures, since they focus on the weakest members of the fleet, while the remainder of the fleet is sound.

In the past two years, ORNL has developed a new Griffith energy-based technique that can provide useful warning of the impending failure of a structure due to end-of-life crack propagation. This technique has been demonstrated by test and analysis in fiberglass composite, aircraft aluminum, and construction steel under pristine and corroded conditions and for Mode I and Mode III fatigue, as well as Mode I low-temperature creep and stress corrosion. Analysis suggests that is should also be valid for flexure and shear loading, Mode II in-plane shear, varying stress amplitudes, and high-temperature creep, although further experimentation will be required to demonstrate this.

2. BACKGROUND

ORNL has developed a nonlinear filtering approach for prediction of an impending structural failure. This method uses energy-consumption methods for crack growth initiation similar to those above. The nonlinear analyses rely on perturbations in strain or strain energy as reliable precursors for crack growth initiated failures. These nonlinear techniques were previously developed and used for predicting epileptic seizures[1-5] and forewarning of drive-train failure in a machining center. The specific nonlinear technology for the present analysis is a novel zero-phase quadratic filter that extracts smooth low-frequency trends in time-serial data, from which we determine trends in hysteresis strain energy (HSE) during fatigue. The relevant data are change in HSE vs number of cycles for fatigue or corrosion fatigue and change in strain energy vs time for creep crack growth or stress corrosion crack growth. The next section explains the methods used.

---

[1]L. M. Hively et al., *Nonlinear Analysis of EEG for Epileptic Seizures*, ORNL/TM-12961, Oak Ridge National Laboratory, April 1995.

[2]N. E. Clapp and L. M. Hively, *Method and Apparatus for Extraction of Low-Frequency Artifacts from Brain Waives for Alertness Detection*, U.S. Patent #5,626,145, May 6, 1997.

[3]L. M. Hively et al., *Apparatus and Method for Epileptic Seizure Detection Using Nonlinear Techniques*, U.S. Patent #5,743,860, April 28, 1998.

[4]L. M. Hively and E. G. Ng, *Integrated Method for Chaotic Time Series Analysis*, U.S. Patent #5,815,413, September 29, 1998.

[5]L. M. Hively et al., *Epileptic Seizure Prediction by Nonlinear Methods*, U.S. Patent #5,857,978, January 12, 1999.

3. ANALYTICAL METHODS

The work consumed by the structure under load is the force-through-a-distance energy, integrated over the work cycle. The force in this case is the applied load, P. We denote the elongation under load as d. Thus, the input strain energy for each cycle is computed as

$$E_{In} = \int_{P_{min}}^{P_{max}} P d\delta \tag{1}$$

over the loading portion of the cycle. The HSE subtracts the strain energy over the unloading part of each cycle from Eq. (1). Thus, HSE is computed as the loop integral

$$HSE = \oint P d\delta \ . \tag{2}$$

The HSE is variable as shown in Fig. 1. HSE depends on load amplitude, material, and other variables. Thus, the value of HSE alone does not predict failure.

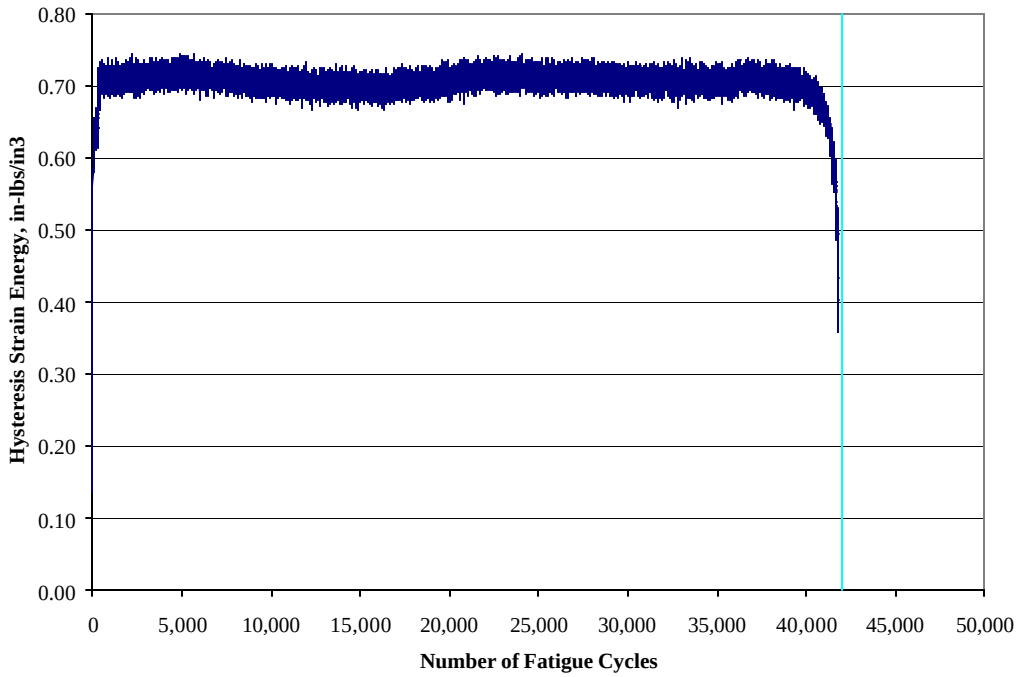

Fig. 1. Example of noise in HSE measurement.

Consequently, we use the slope of HSE vs number of cycles and the curvature of HSE vs number of cycles as leading indicators of trends in HSE. To accomplish this, we extract smooth trends with a novel, zero-phase, quadratic filter. This filter uses a moving window of 2w + 1 points of HSE(N) data, with the same number of data samples (w) on either side of the central point. We estimate the trend (y) at the central point of this window from a quadratic regression of the 2w + 1 points. We find that a filter window width for adequate smoothing is w = 5% of the total number of loading cycles. The smoothed trend then has the form, $y(z) = az^2 + bz + c$. Here, z = N – n, with n as the (fixed) value of the number of loading cycles associated with the central point in the filter window. The corresponding value of y(z) at the central point of the window is y(z = 0) = c. The slope at the central point is $y'(z = 0) = b$. The second derivative at the central point of the window is $y''(z = 0) = 2a$. The curvature of the curve $y(z)$ is defined as:

$$\kappa = \frac{y''}{[1+(y')^2]^{3/2}} \quad . \tag{3}$$

Experimental data shows that considerable low-amplitude variation still exists in the slope and curvature even after this filtering process. Consequently, we distinguish random variations from a systematic trend to detect failure onset. We make this distinction by treating the values of slope and curvature as statistical variables. This idea is similar to that for which an industrial process control chart is constructed. In the subsequent analysis, $\underline{x}$ denotes the sample mean, which is computed from the beginning of the data to the current cycle:

$$\overline{x} = \frac{\sum_{i=1}^{n} x_i}{n} . \tag{4}$$

The corresponding standard deviation estimate (s) is obtained from

$$s^2 = \frac{\sum_{i=1}^{n} \left(x_i - \overline{x}\right)^2}{\left(N-1\right)} . \tag{5}$$

We define an indication of failure onset as the point when the slope (or curvature) rises above the upper control limit (UCL) or falls below the lower control limit (LCL). These values are defined as:

$$\begin{aligned} UCL &= \overline{x} + 4s \, , \\ LCL &= \overline{x} - 4s. \end{aligned} \tag{6}$$

The probability of Gaussian random data exceeding one of these limits corresponds to a false positive probability of 1 part in 31,574 measurements (cycles). Subsequent sections describe our tests in the context of this analytical approach.

4. INITIAL EXPERIMENTS

4.1 OBJECTIVE

A series of experiments recorded tensile load, grip displacement, and tensile strain on four coupons with expected fatigue lifetimes in the 1,000 to 10,000 cycle range. We then calculated the HSE strain being consumed by the coupon using the tensile load and tensile strain over a 1-in. gage length during each fatigue cycle. We applied nonlinear mathematical techniques to the prediction of imminent fatigue failure using the techniques described in Section 4.

4.2 METHOD

The coupon material is a randomly oriented fiber-reinforced plastic that is part of an ORNL test program for next-generation automotive vehicles. The coupons were nominally 1/8-in. thick and were machined to an ORNL-designed reduced cross-sectional shape with a 1.6-in. gage section for the 1-in. extensometer.

Three data variables were recorded from the experiment—displacement of the loading grips, tensile load, and tensile strain in the reduced section as measured by an extensometer. Loading was performed on a servohydraulic test machine of 10,000 lb capacity and at room temperature. The fatigue loading frequency was 10 Hz. Data were recorded by a National Instruments PCI 16XE-50 General Purpose I/O System of 16-bit resolution. The data recording frequency was 2000/channel/s, producing ~200 measurements of each variable over each fatigue cycle. Load cell voltage variations were of the order of 0.1% (10 mV) of full scale (10 V), or 10 lb. Measurement resolution was 1 lb in load measurement (~10 psi) and 5 με in strain measurement.

4.3 TEST RESULTS

The fatigue test results for the four coupon samples tested are shown in Table 1 and the following figures.

4.4 DATA ANALYSIS

Graphs of hysteresis fatigue strain energy per cycle vs the number of cycles with a vertical bar indicating the point of failure are shown below in Figs. 2–5 for specimens P36-O-45, P36-O-46, P36-O-47, and P36-O-48, respectively.

Table 1. Fatigue test results

	Specimen			
	P36-O-45	**P36-O-46**	**P36-O-47**	**P36-O-48**
Cross-sectional area, in.^{2}	0.0996	0.0993	0.1003	0.0894
Nominal peak tensile load, lb	1,480	1,478	1,190	1,188
Nominal peak tensile stress, psi	14,860	14,885	11,865	13,290
Nominal minimum tensile load, lb	140	147	121	116
Nominal minimum tensile stress, psi	1,406	1,480	1,206	1,298
Cycles to failure	3,686	2,417	24,506	5,763

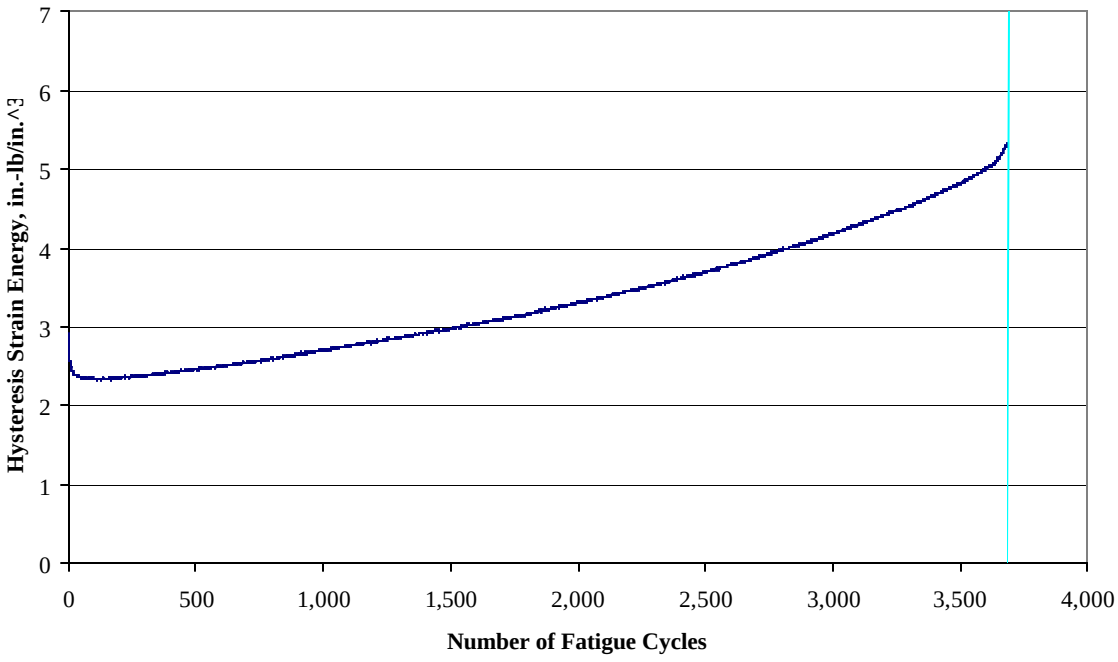

Fig. 2. HSE vs number of fatigue cycles, unnotched fiberglass sample P36-O-45.

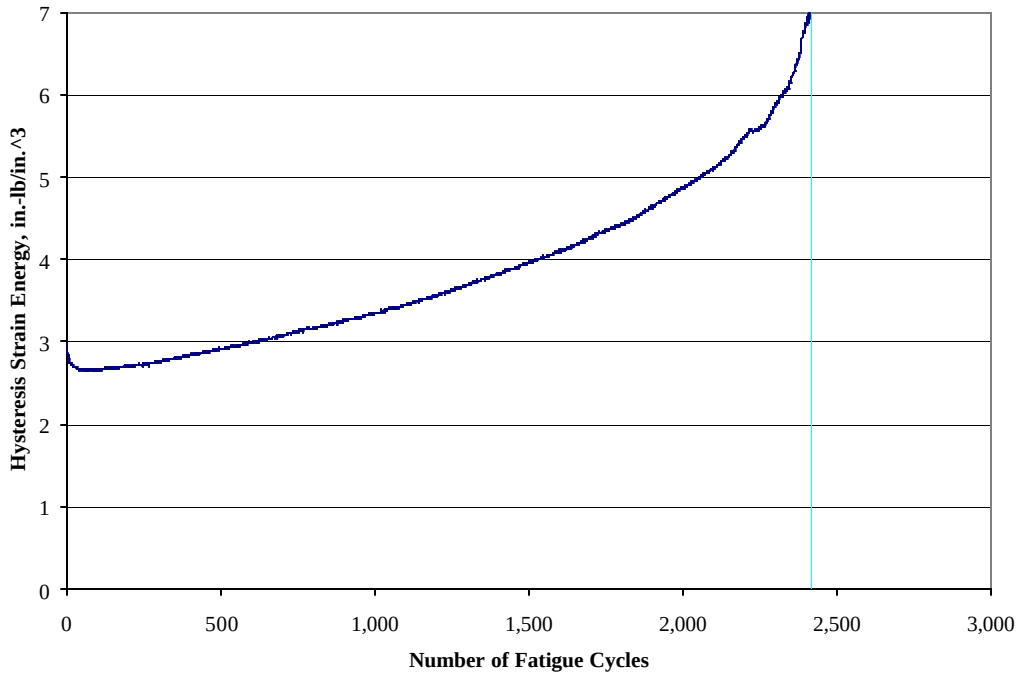

Fig. 3. HSE vs number of fatigue cycles, unnotched fiberglass sample P36-O-46.

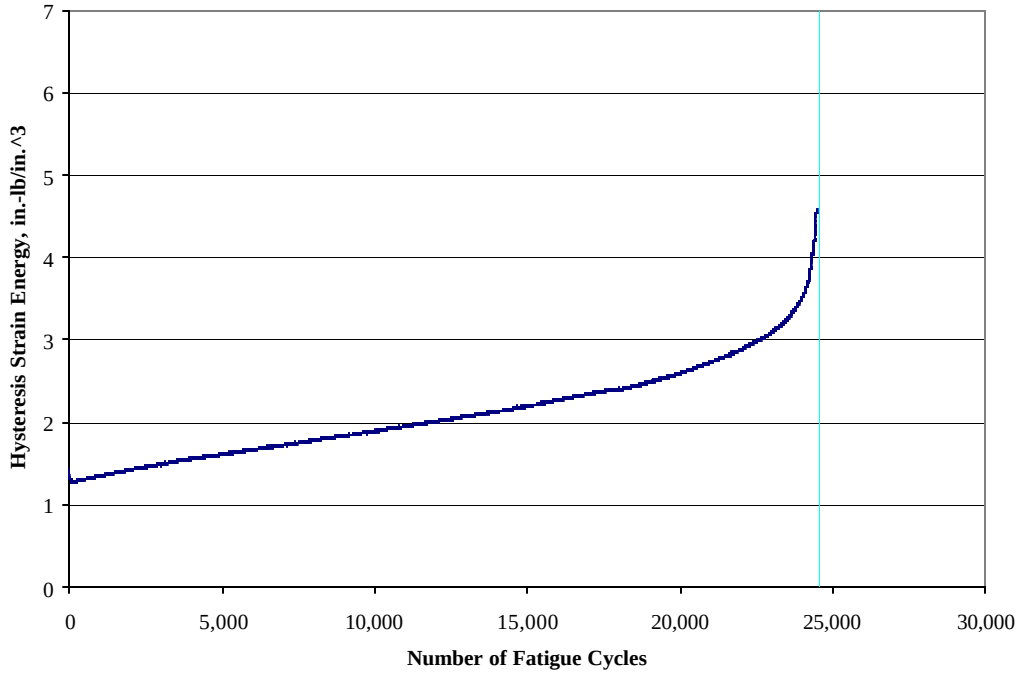

Fig. 4. HSE vs number of fatigue cycles, unnotched fiberglass sample P36-O-47.

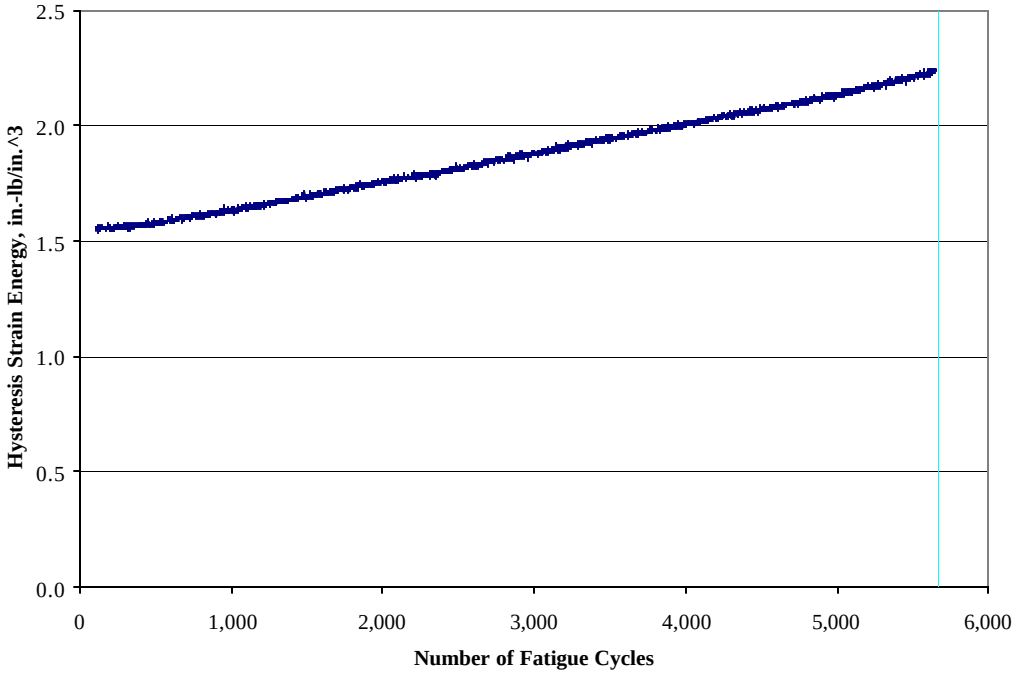

Fig. 5. HSE vs number of fatigue cycles, unnotched fiberglass sample P36-O-48.

These figures show that the initial HSE consumption per fatigue cycle is approximately 1.5 to 3 in.-lb/in.^{3}, initially decreasing sharply (although not visible in Fig. 3 due to the plotting scale), then rising monotonically, and finally rising suddenly near failure. In attempting to determine a criterion that would indicate impending failure, it was decided that the criterion should first allow for the uniformly observed period of HSE decrease seen in the first few cycles for all samples.

However, after this initial minimum, the actual level of HSE does not seem to be a suitable criterion, because the HSE depends on the loading and strain energy amplitude of the cycle, which varied among the four specimens. A better criterion is the slope of the HSE per cycle vs the number of cycles because this indicates how quickly the energy consumption is rising. However, the value of the slope of HSE vs the number of cycles does not represent a uniform criterion of impending fatigue failure. The slope of a fitted quadratic to these curves is shown below in Figs. 6–9 for specimens P36-O-45, P36-O-46, P36-O-47, and P36-O-48, respectively.

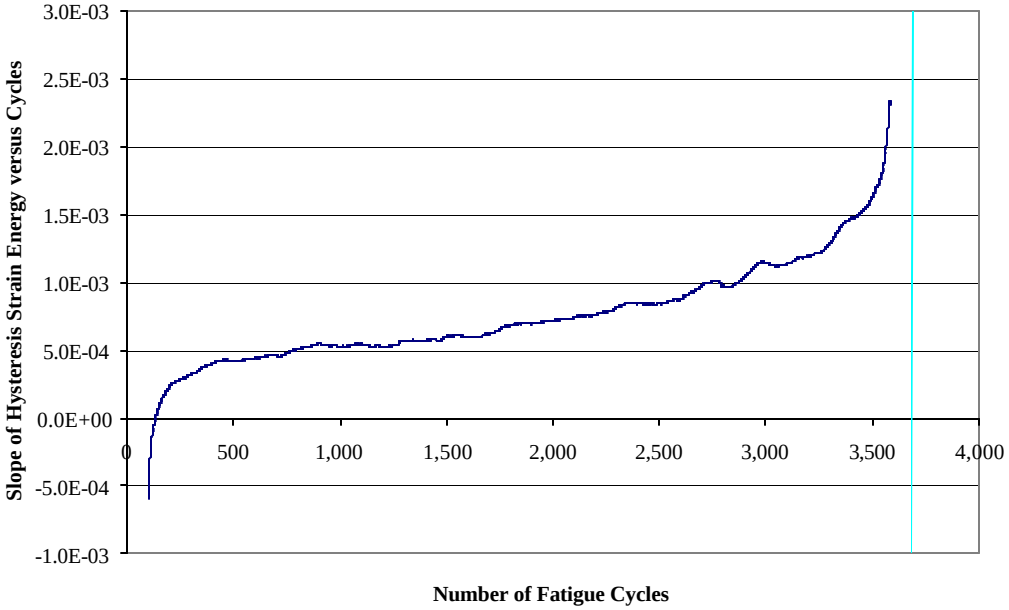

Fig. 6. HSE vs fatigue cycles, sample P36-O-45.

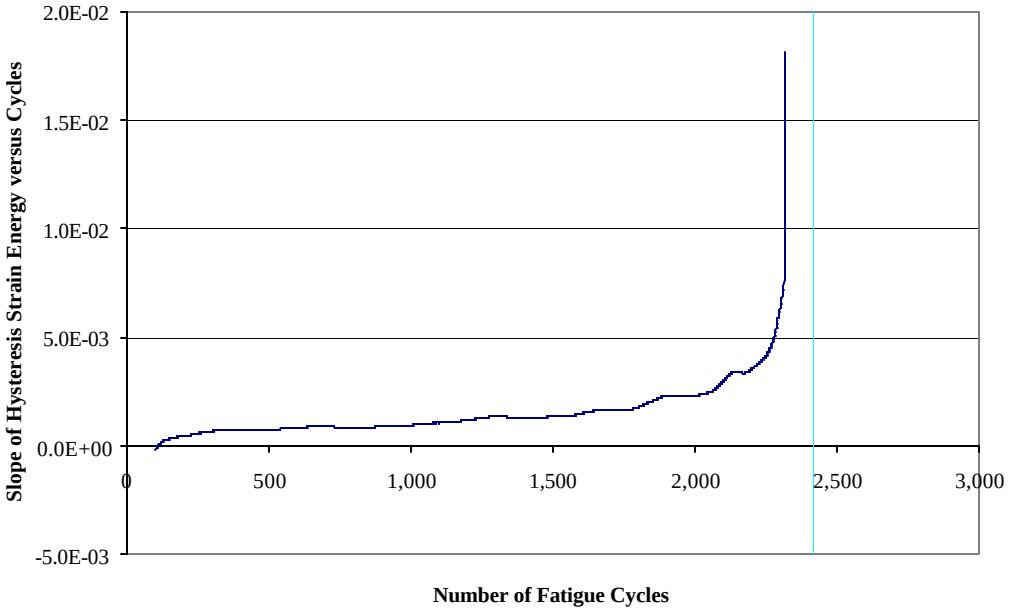

Fig. 7. HSE vs fatigue cycles, sample P36-O-46.

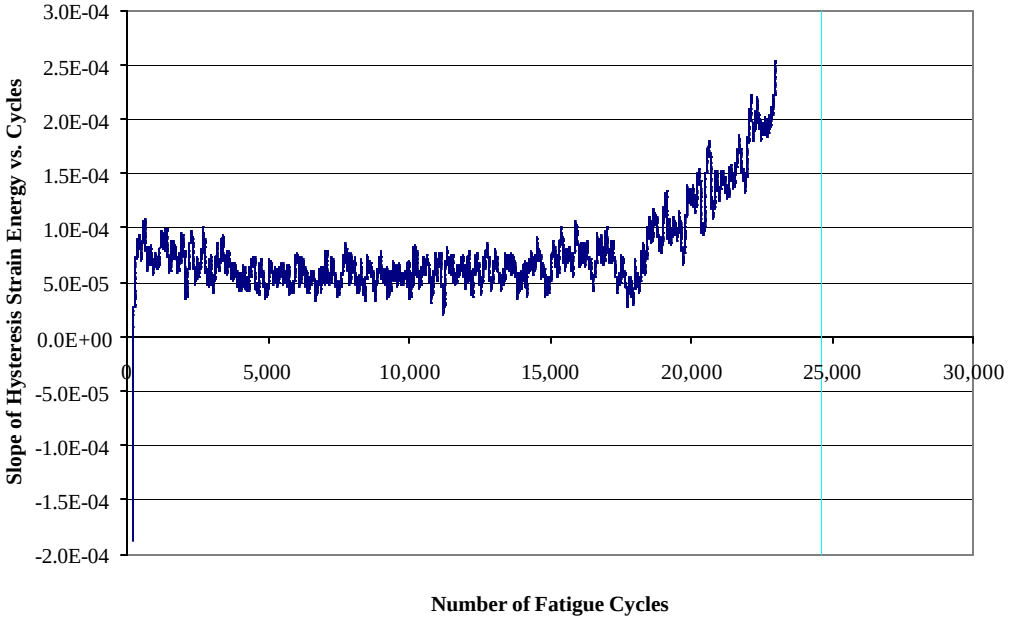

Fig. 8. Slope of HSE vs fatigue cycles, sample P36-O-47.

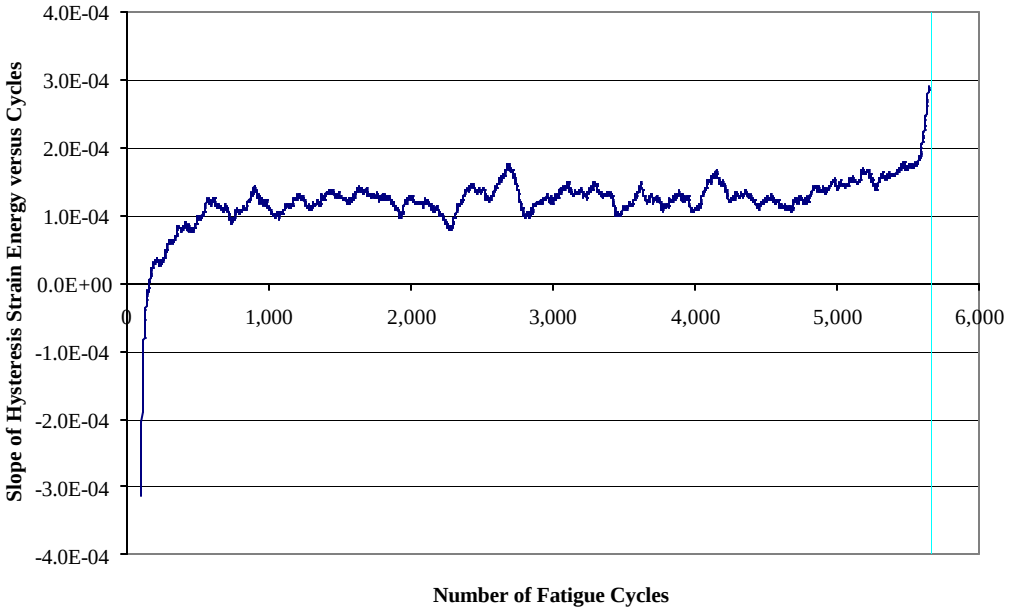

Fig. 9. Slope of HSE vs fatigue cycles, sample P36-O-48.

Figures 2–5 show some small amplitude noise in the HSE vs the number of cycles data, especially on the lower stress specimens. These small amplitude variations are magnified as successive derivatives of the curve are taken.

The curvature data for the specimens are shown in Figs. 10–13 for specimens P36-O-45, P36-O-46, P36-O-47, and P36-O-48 respectively.

Figures 10–13 show a greater degree of advance warning of impending fatigue failure by the curvature of the HSE curve as compared to the HSE curve itself.

However, there is a considerable amount of low-amplitude variation in the curvature. We distinguish the sudden rise in curvature at the end of fatigue life from the low-amplitude variations by treating the value of the curvature as a statistical variable similar to that for which an industrial process control chart is constructed. The curvature was plotted, along with a UCL and LCL, as discussed previously.

Assuming that an excursion above the UCL or below the LCL will be taken as an indication of impending failure, than a 4s limit will lead to a probability of randomly exceeding in UCL of 1 in 31,560 measurements. Because the number of cycles measured for specimen P36-O-47 is 24,405, this value is appropriate to minimize the occurrence of a false positive indication. The value of the UCL and LCL may be selected to minimize the probability of a false positive indication while avoiding a false negative indication (failing to indicate an impending failure).

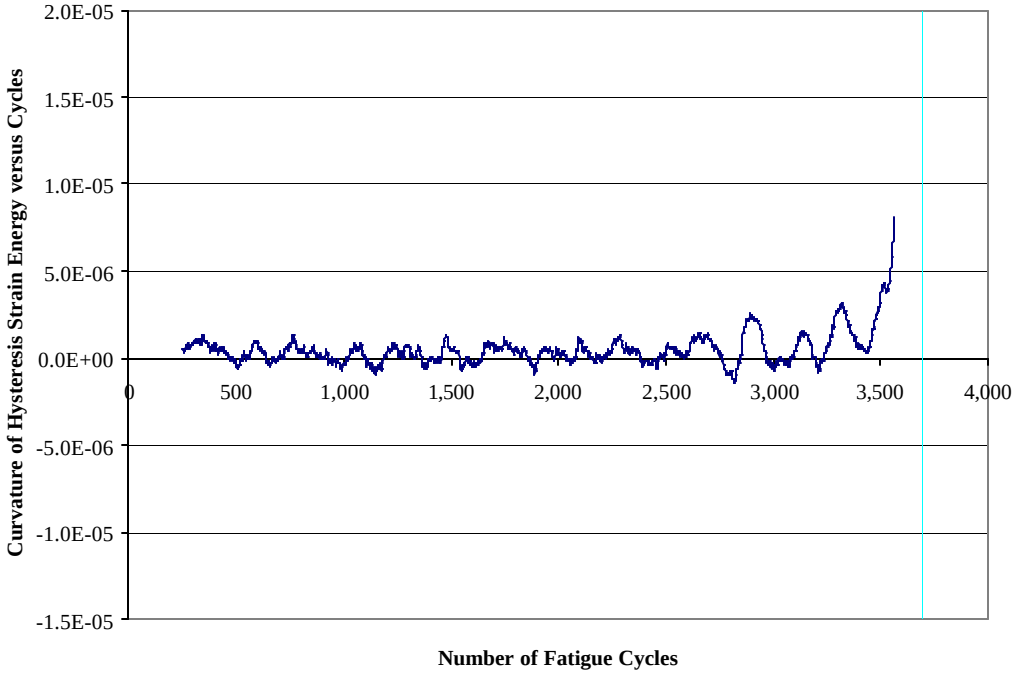

Fig. 10. Curvature of HSE vs fatigue cycles, sample P36-O-45.

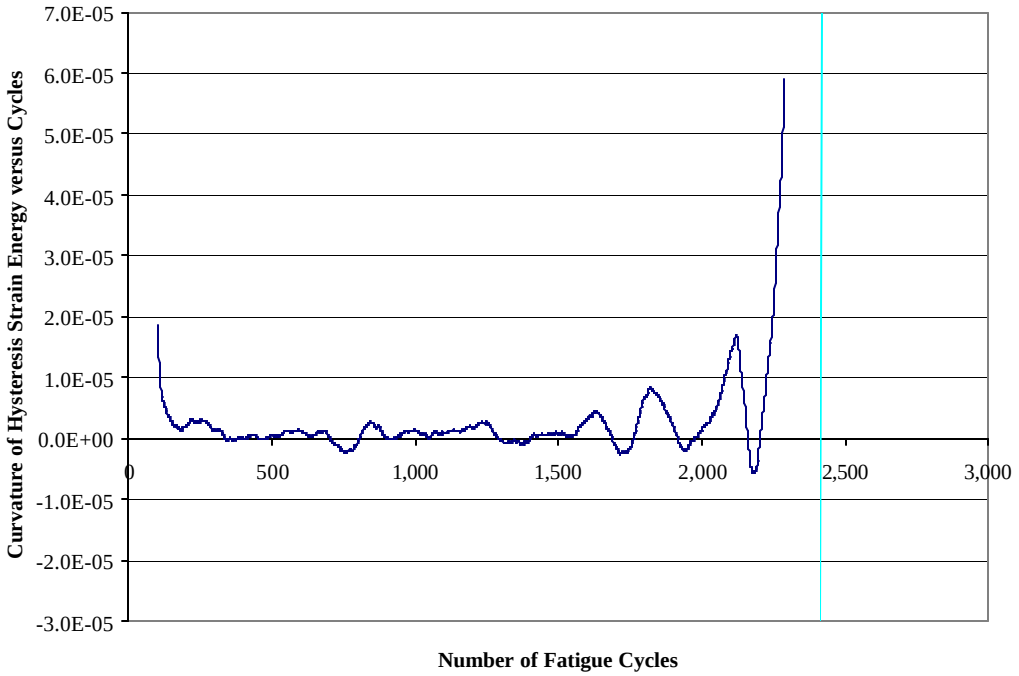

Fig. 11. Curvature of HSE vs fatigue cycles, sample P36-O-46.

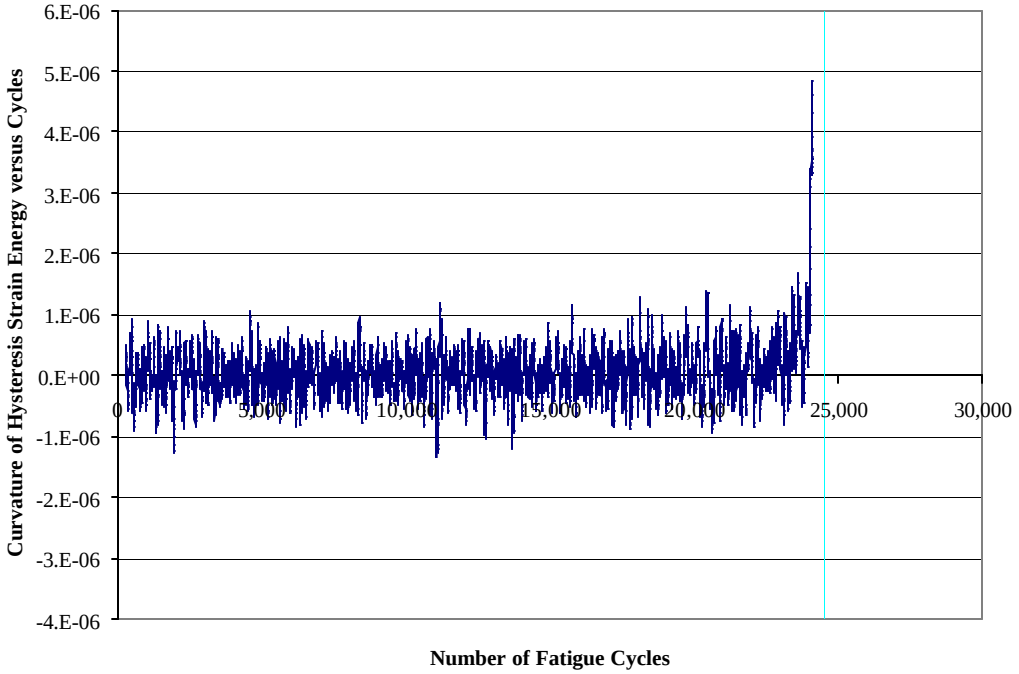

Fig. 12. Curvature of HSE vs fatigue cycles, sample P36-O-47.

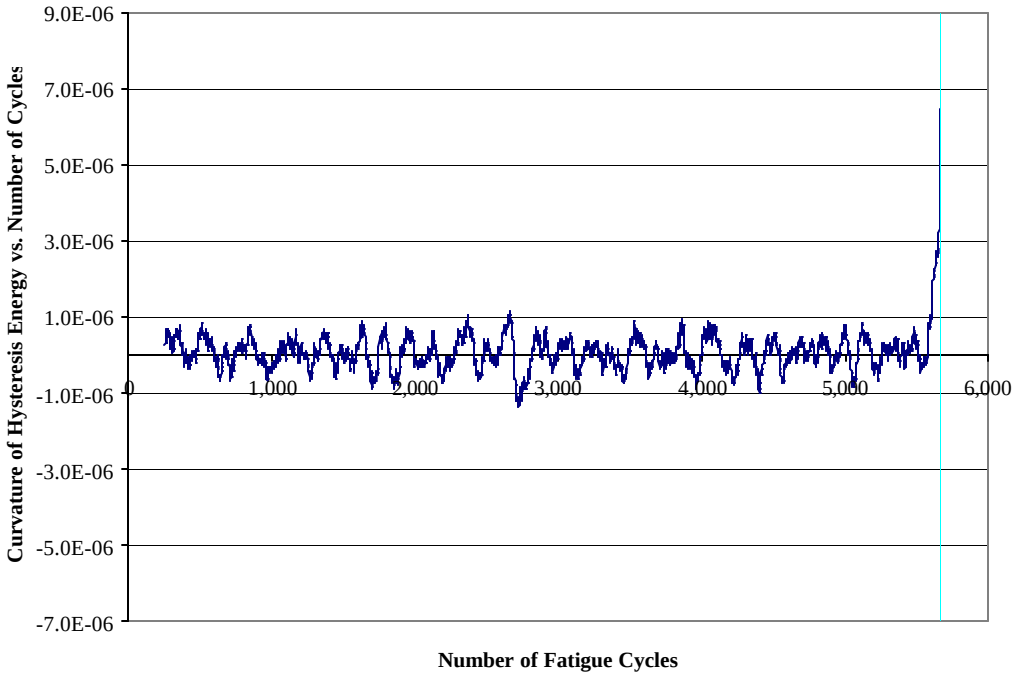

Fig. 13. Curvature of HSE vs fatigue cycles, sample P36-O-48.

Figures 14–17 shows the smoothed slope of HSE vs the number of cycles plotted with the LCL and UCL calculated point by point as the data progress.

Figures 18–21 shows the average curvature data in Figs. 10–13. Figures 18–21 also include the LCL and UCL calculated point by point as the data progress.

In addition, Figs. 18–21 show that excursions in average curvature above the UCL are another predictor of impending fatigue failure.

When the slope and curvature indicators of imminent fatigue failure are combined, forewarnings are given as shown in Table 2.

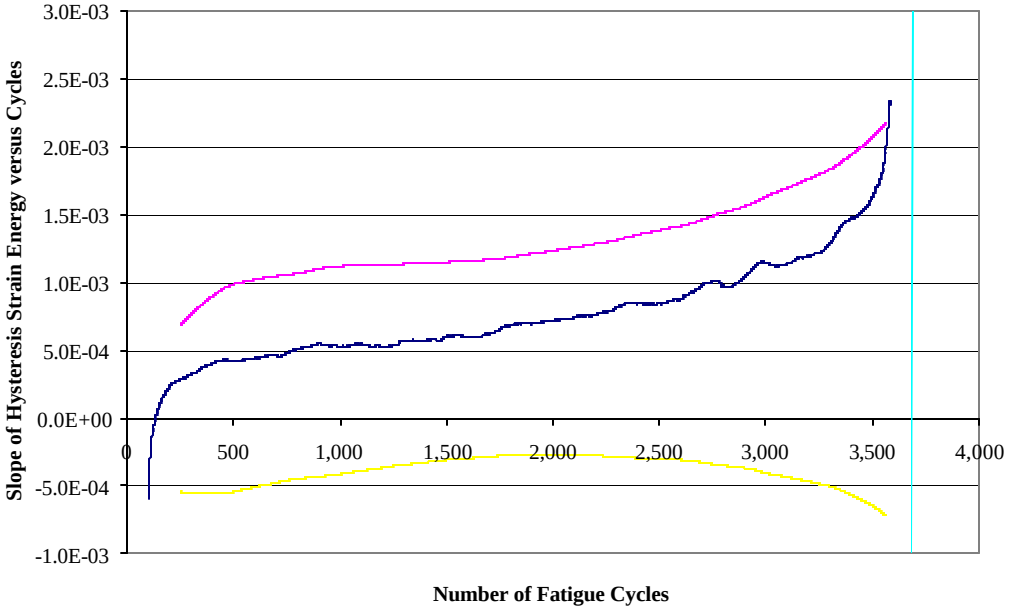

Fig. 14. Slope of HSE vs cycles with UCL and LCL, unnotched fiberglass sample P36-O-45.

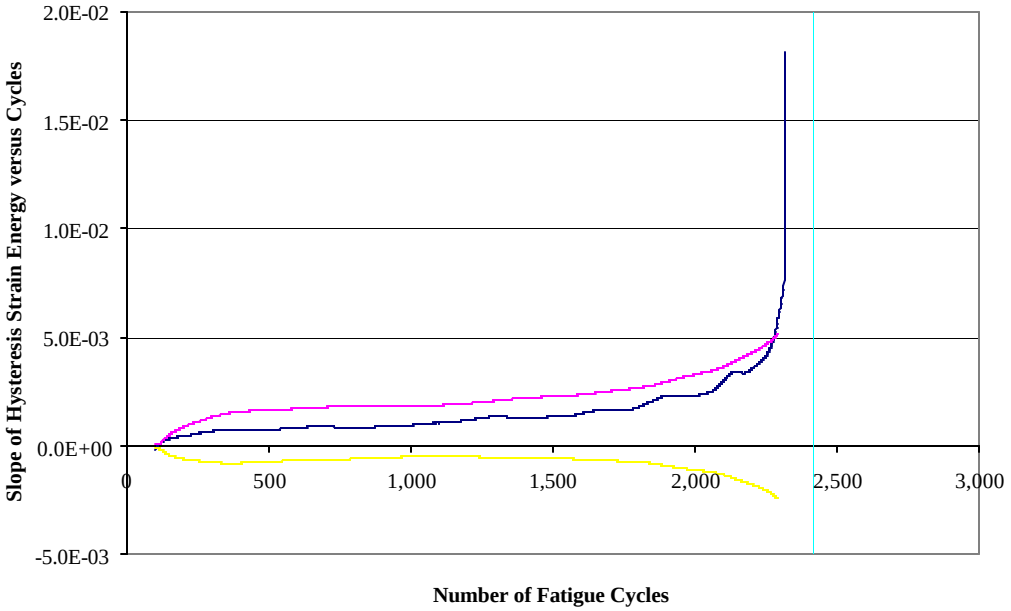

Fig. 15. Slope of HSE vs cycles with UCL and LCL, unnotched fiberglass sample P36-O-46.

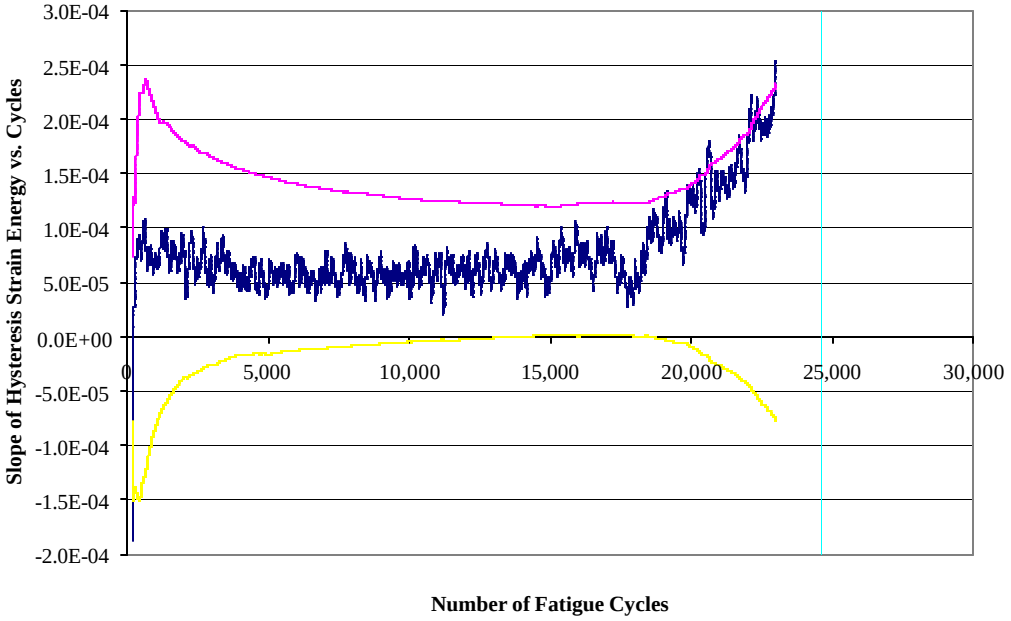

Fig. 16. Slope of HSE vs cycles with UCL and LCL, unnotched fiberglass sample P36-O-47.

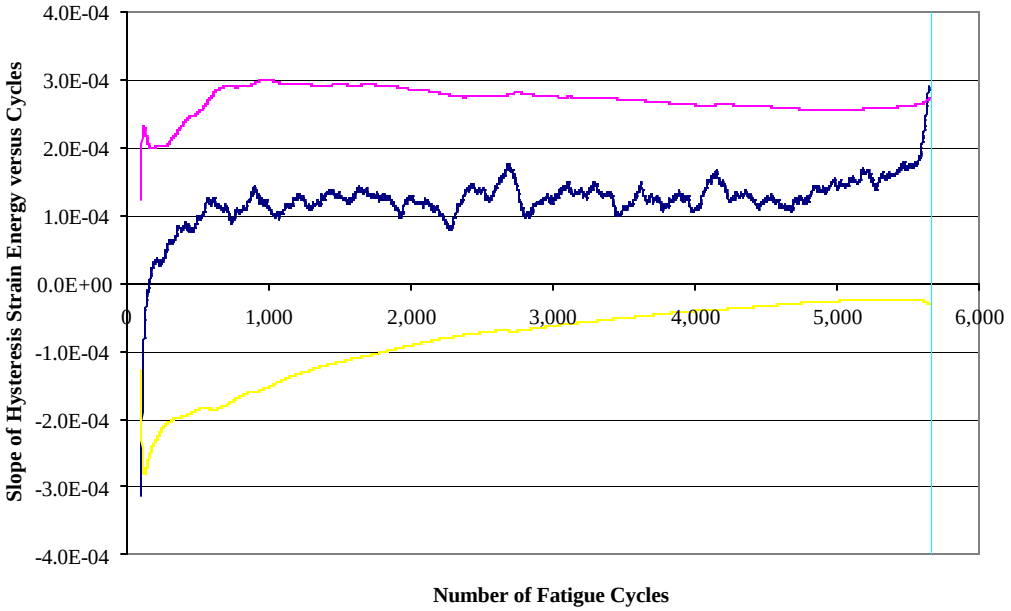

Fig. 17. Slope of HSE vs cycles with UCL and LCL, unnotched fiberglass sample P36-O-48.

.

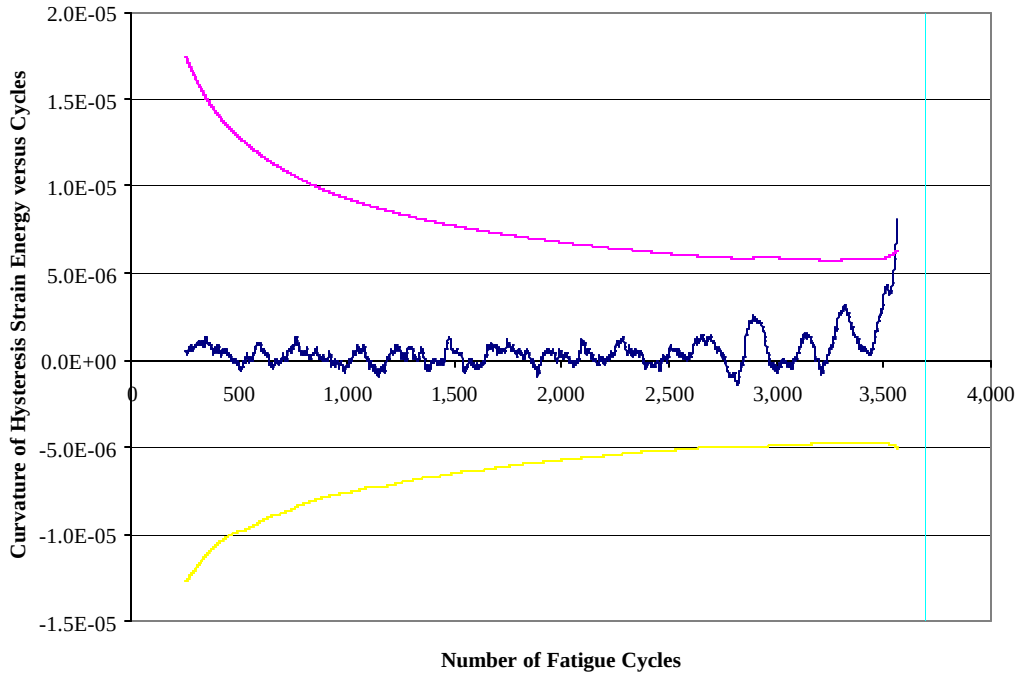

Fig. 18. Curvature of HSE vs cycles with UCL and LCL, unnotched fiberglass sample P36-O-45.

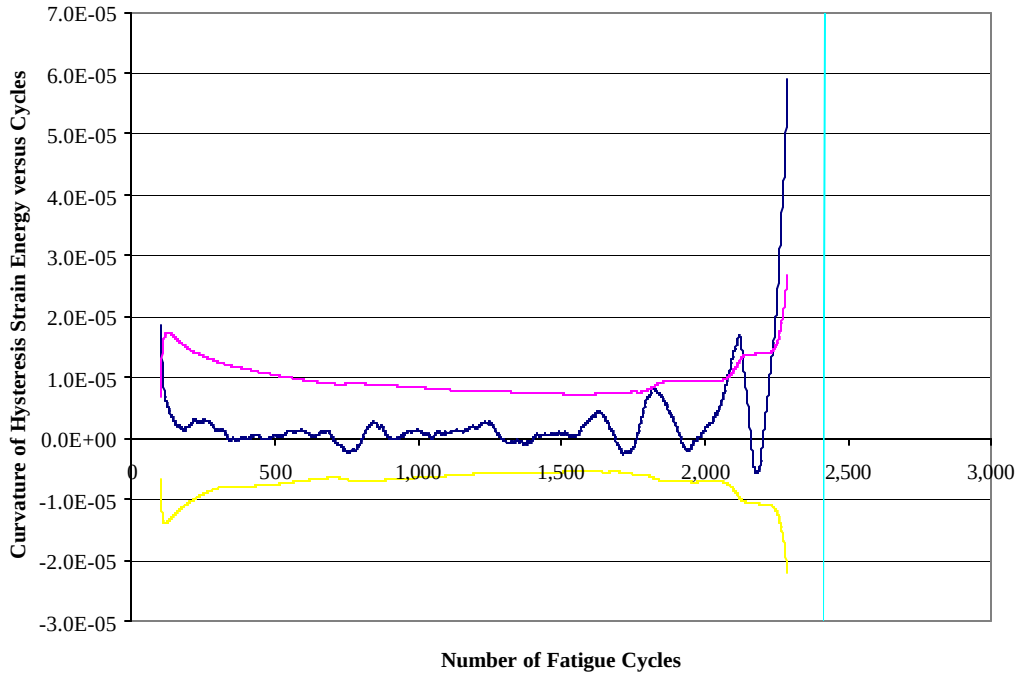

Fig. 19. Curvature of HSE vs cycles with UCL and LCL, unnotched fiberglass sample P36-O-46.

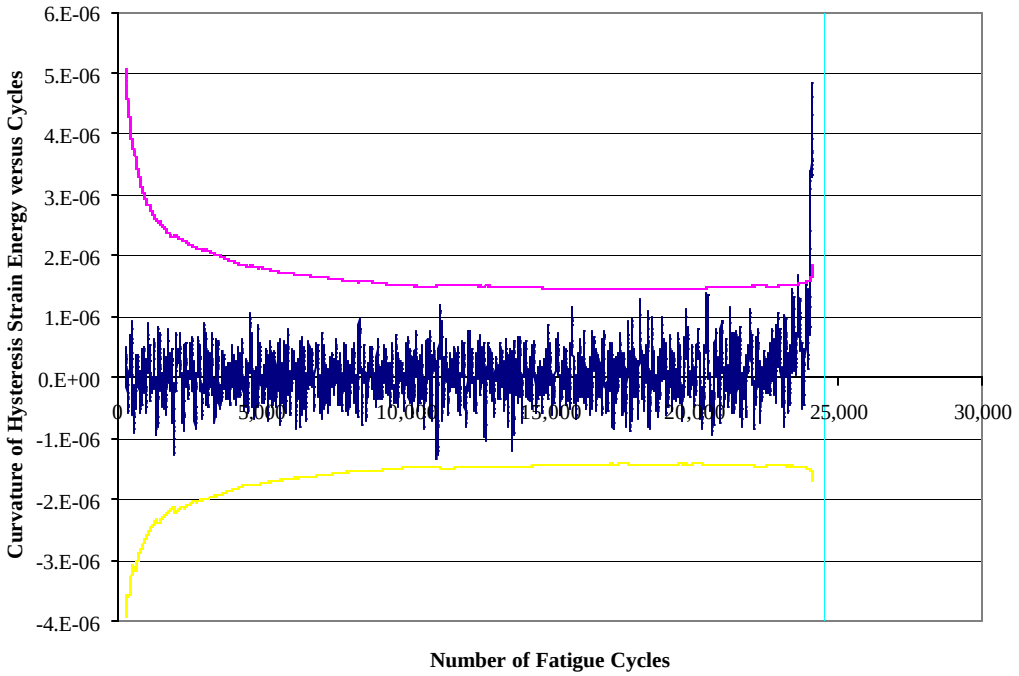

Fig. 20. Curvature of HSE vs cycles with UCL and LCL, unnotched fiberglass sample P36-O-47.

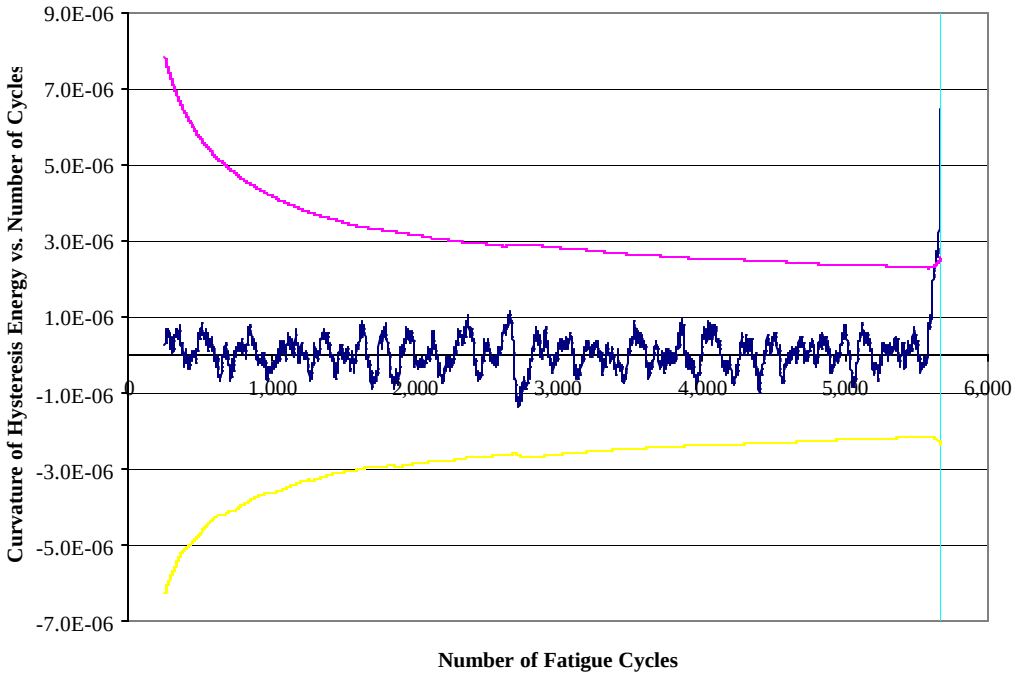

Fig. 21. Curvature of HSE vs cycles with UCL and LCL, unnotched fiberglass sample P36-O-48.

Table 2. Number of fatigue cycles where slope or curvature exceeds UCL with remaining fatigue life

	Specimen			
	P36-O-45	**P36-O-46**	**P36-O-47**	**P36-O-48**
Cycles for slope or curvature > UCL	2,888	1,896	19,082	5,706
Indication based on slope or curvature	Curvature	Curvature	Curvature	Slope
Cycles to failure	3,686	2,417	24,506	5,763
Fatigue life remaining after indication, %	21.65	21.56	22.13	0.99

5. PHASE I EXPERIMENTS

5.1 OBJECTIVE

A series of experiments recorded tensile load and tensile strain on ten aircraft aluminum coupons with expected fatigue lifetimes in the 10,000 to 100,000 cycle range. The HSE being consumed by the coupons during each fatigue cycle was calculated. Then, the nonlinear methods of Sect. 4 were applied to the prediction of imminent fatigue failure.

5.2 METHOD

The coupon material is an unclad 2024-T3 aluminum alloy sheet, a material commonly used in aircraft skins. The coupons were made to model the outer skin of the U.S. Air Force KC-135, which is nominally 0.090-in. thick. They were machined to an ASTM E466 standard fatigue specimen with reduced cross-sectional width with a 1.3-in.-long by ½-in.-wide gage section for the 1-in. extensometer.

The two data variables recorded from the experiment were tensile load and tensile strain in the reduced section as measured by an extensometer. Loading was performed on a servohydraulic test machine of 10,000 lb capacity and at room temperature. The fatigue loading frequency was 10 Hz. Data were recorded by a National Instruments PCI 16XE-50 General Purpose I/O System of 16-bit resolution. The data recording frequency was approximately 4000/channels, producing ~400 measurements of each variable over each fatigue cycle. Load cell voltage variations were of the order of 0.1% (10 mV) of full scale (10 V), or 10 lb. Measurement resolution was 1 lb in load measurement (~10 psi) and 5 Fe in strain measurement.

5.3 TEST RESULTS

An initial stress-strain curve for a test sample of the 2024-T3 aluminum material was obtained and is shown in Fig. 22. Figure 23 is a future illustrating the deviation from true linearity of the stress-strain response of this specimen on a cycle-by-cycle basis, which illustrates HSE phenomena.

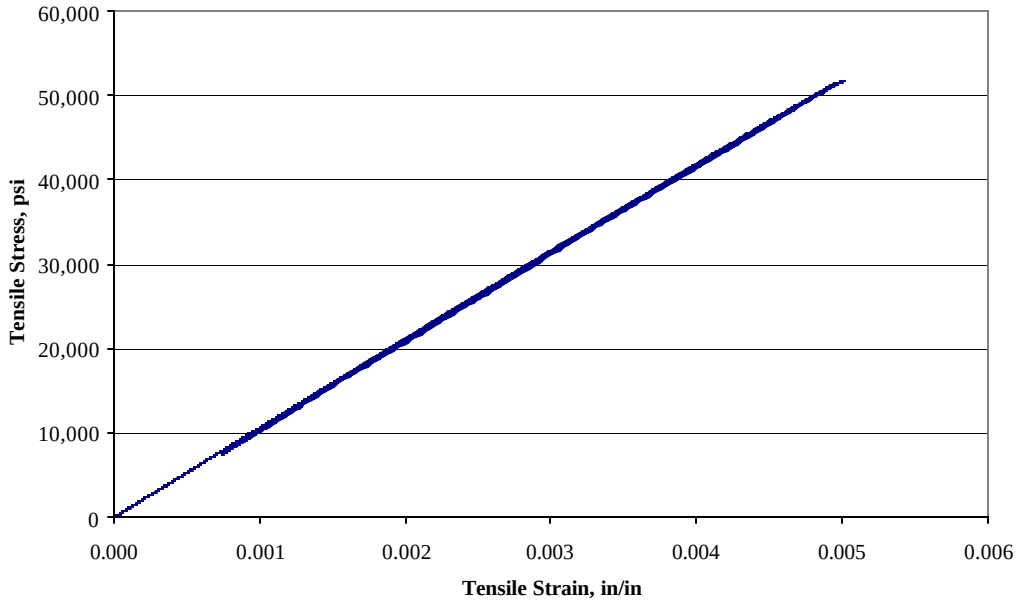

Fig. 22. Initial stress-strain response of 2024-T3 aluminum unnotched uncorroded sample.

Appendix B shows Figs. B-1 thru B-40 for the ten coupon samples tested (all 0.045-in.^{2} cross-sectional area), and the resulting data are also shown in Table 3.

Table 3. Fatigue test results

	Specimen									
	TM-1	**TM-2**	**TM-3**	**TM-4**	**TM-5**	**TM-6**	**TM-7**	**TM-8**	**TM-9**	**TM-10**
Nominal peak tensile load, lb	2,340	2,340	2,340	2,340	2,340	2,340	2,340	2,760	3,000	3,120
Nominal peak tensile stress, psi	52,000	52,000	52,000	52,000	52,000	52,000	52,000	61,340	66,629	71,917
Nominal minimum tensile load, lb	234	234	234	234	234	234	234	276	300	312
Nominal minimum tensile stress, psi	5,200	5,200	5,200	5,200	5,200	5,200	5,200	6,134	6,663	7,192
Cycles to failure	33,133	41,955	25,404	43,750	44,727	39,969	34,682	17,142	12,362	6,938
Cycles of fatigue life remaining after indication	538	738	419	357	578	972	1,656	578	213	122
Fatigue life remaining after indication, %	1.62	1.76	1.65	0.82	1.29	2.43	4.78	3.37	1.72	1.76

5.4 DATA ANALYSIS

Graphs of the input strain energy and the HSE per cycle vs the number of cycles are shown in Figs. B-5, B-9, B-13, B-17, B-21, B-25, and B-29 for specimens TM-2 to TM-7, respectively, and Figs. B-2, B-6, B-10, B-14, B-18, B-22, B-26, and B-30 for specimens TM-1 to TM-7 in Appendix B. The input strain energy curve for sample TM-1 was not available as its computation was only performed on later samples.

When the calculated slope and curvature indicators of imminent fatigue failure are combined, forewarnings are given as shown in Table 4.

Table 4. Combined indicators of imminent fatigue failure

	Specimen									
	TM-1	**TM-2**	**TM-3**	**TM-4**	**TM-5**	**TM-6**	**TM-7**	**TM-8**	**TM-9**	**TM-10**
Indication based on:	Curv.	Slope	Slope	Slope	Slope	Slope	Curv.	Slope	Slope	Curv.
Cycles for indication >	32,59	41,21	24,98	43,39	43,94	38,99	33,02	16,56	12,14	

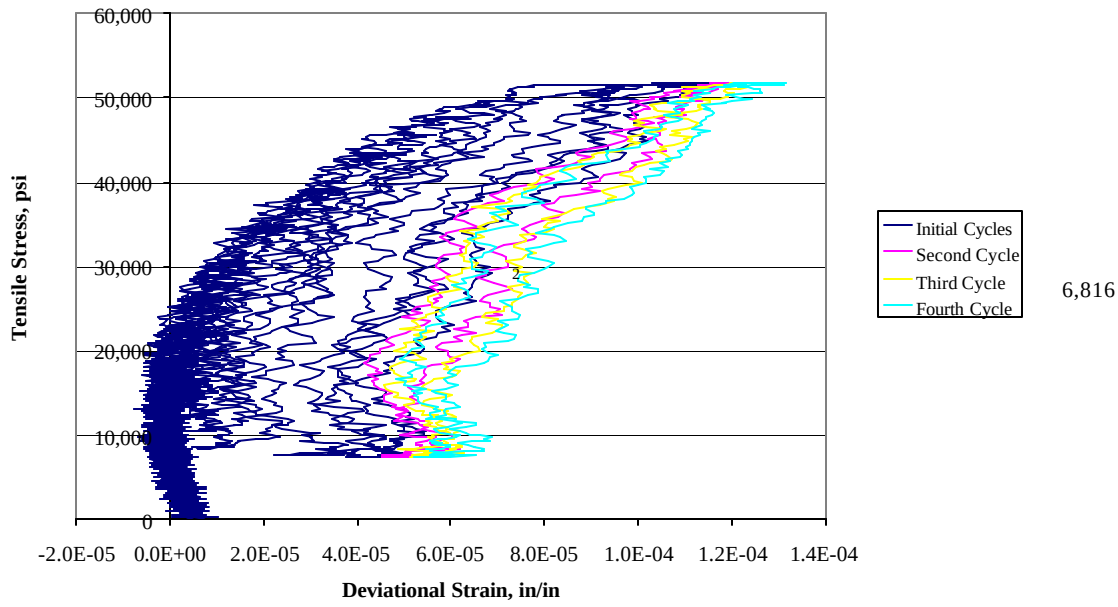

Fig. 23. Fatigue stress vs deviational strain, unnotched uncorroded 2024-T3 aluminum sample.

UCL or < LCL	5	7	5	3	9	7	6	4	9

6,816

Cycles to failure	33,133	41,955	25,404	43,750	44,727	39,969	34,682	17,142	12,362	6,938
Cycles of life remaining after indication	538	738	419	357	578	972	1,656	578	213	122
Fatigue life remaining after indication, %	1.62	1.76	1.65	0.82	1.29	2.43	4.78	3.37	1.72	1.76
Position of failure surface relative to extensometer midspan, 0% = midspan , 100% = span edge	175%	175%	0%	100%	100%	150%	125%	—	—	—
Sense of initial HSE change	Falls	Falls	Falls	Falls	Falls	Rises	Rises	Falls	Falls	Falls

The measured position of the failure surface relative to the extensometer range was plotted and is shown in Fig. 24 below.

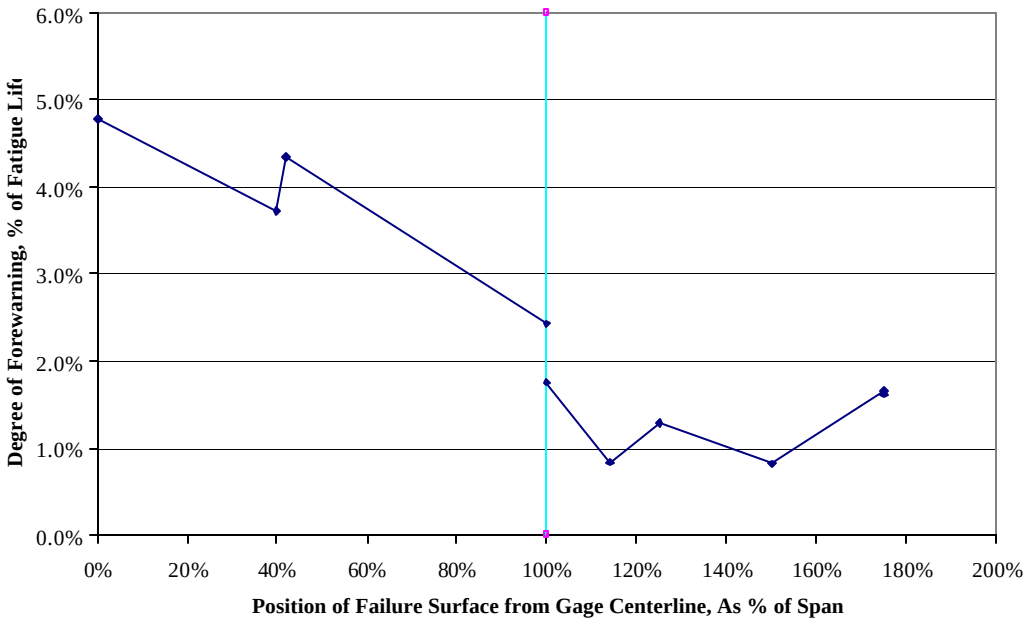

Fig. 24. Variation of degree of forewarning vs location of failure surface relative to displacement gage midspan.

6. PHASE II EXPERIMENTS

6.1 OBJECTIVE

A series of experiments was designed to record tensile load and tensile strain on three classes of specimens. They are (1) tension-tension-loaded aluminum coupons designed to simulate MSD situations by containing a single drilled hole in the center of the gage section, (2) flexure-flexure loaded I-beam samples in a four-point bend test, and (3) tensile-loaded single lap shear loaded coupons. The HSE being consumed by each sample during each fatigue cycle would then be calculated. Then, nonlinear techniques of Sect. 3 are then applied to the prediction of approaching fatigue failure.

6.2 METHOD

The sample material for the tension-tension aluminum coupon is an unclad 2024-T3 aluminum alloy sheet 0.090-in. thick, a material commonly used in aircraft skins. The coupons were machined to an ASTM E466 standard fatigue specimen with cross-sectional dimensions of 0.5-in.-wide by 1.22-in.-long gage section for the 1-in. extensometer used. To simulate a proof of principle MSD situation, a single No. 55 drilled hole (0.052-in.-diam.) was drilled in the center of each specimen's gage section.

Two data variables were recorded from the experiment—tensile load and tensile strain in the reduced section as measured by the extensometer. Loading was performed on a servohydraulic test machine of 10,000 lb capacity, at room temperature. The fatigue loading frequency was 10 Hz. Data were recorded by a National Instruments PCI 16XE-50 General Purpose I/O System of 16-bit resolution. The data recording frequency was approximately 2000/channel/s, producing ~200 measurements of each variable over each fatigue cycle. Load cell voltage variations were of the order of 0.1% (10 mV) of full scale (10 V), or 10 lb. Measurement resolution was 1 lb in load measurement (~10 psi) and 5 με in strain measurement.

6.3 TEST RESULTS

These specimens were numbered TM2-MSD-1 through TM2-MSD-8 (all had cross-sectional areas of 0.045 $in.^2$. These specimens were fatigue tested in tension at R = 0.1 and at the peak nominal stresses shown below in Table 5.

The strong dependence of the plateau value of the HSE on stress level was noted, and suggests further experiments. A stress-strain curve for the material in the L-T configuration was obtained from the first loading cycle of previously tested specimen TM-10. This curve is shown in Fig. 22.

A ninth MSD specimen, TM2-MSD-9, was prepared and tested at various stress levels.

6.4 DATA ANALYSIS

Graphs of the input strain energy and the HSE per cycle vs the number of cycles are shown in Appendix C, Figs. C-1, C-5, C-9, C-13, C-17, C-21, C-25, and C-29. Specimens for TM2-MSD-1 to TM2-MSD-8 are shown respectively in Figs. C-2, C-6, C-10, C-14, C-18, C-22, C-26, and C-30.

As may be seen from these figures, the initial HSE consumption per fatigue cycle varies from approximately 0.07 in.-lb for 17,333 psi to 0.92 in.-lb for 52,000 psi to 0.62 in.-lb for 44,444 psi to 0.3 for 33,333 psi. The HSE is more or less constant until it falls sharply at failure. In attempting to determine a criterion that would indicate impending failure, we decided that the actual level of HSE does not seem to be a suitable criterion because HSE depends on the loading and strain energy amplitude of the cycle, which varied among the eight specimens.

Table 5. Fatigue test results

	Specimen								
	MSD-1a	**MSD-1b**	**MSD-2**	**MSD-3**	**MSD-4**	**MSD-5**	**MSD-6**	**MSD-7**	**MSD-8**
Nominal peak tensile load, lb	780	2,340	2,000	2,000	2,000	2,000	1,500	1,500	1,500
Nominal peak tensile stress, psi	17,333	52,000	44,444	44,444	44,444	44,444	33,333	33,333	33,333
Nominal minimum tensile load, lb	78	234	200	200	200	200	150	150	150
Nominal minimum tensile stress, psi	1,733	5,200	4,444	4,444	4,444	4,444	3,333	3,333	3,333
Cycles to failure	No fail at 10^5	2,550	6,888	5,829	7,923	7,891	27,008	24,180	31,795
Cycles of fatigue life remaining after indication		205	649	833	817	1,138	3,307	2,441	3,769
Indication based on slope or curvature		Slope	Slope	Slope	Curv.	Curv.	Curv.	Curv.	Curv.
Fatigue life remaining after indication, %		8.04	9.42	14.29	10.31	14.42	12.24	10.10	11.85
HSE plateau value	0.07	0.92	0.67	0.62	0.63	0.62	0.31	0.31	0.32

A better criterion is the slope of the HSE per cycle vs the number of cycles because this indicates how quickly the energy consumption is rising. We reduced the effect of noise[1–3] on the slope and curvature

[1]L. M. Hively et al., *Nonlinear Analysis of EEG for Epileptic Seizures*, ORNL/TM-12961, Oak Ridge National Laboratory, April 1995.

[2]N. E. Clapp and L. M. Hively, *Method and Apparatus for Extraction of Low-Frequency Artifacts from Brain Waives for Alertness Detection*, U.S. Patent #5,626,145, May 6, 1997.

[3]L. M. Hively et al., *Apparatus and Method for Epileptic Seizure Detection using Nonlinear Techniques*,

data by fitting a quadratic equation to the HSE curve over a 200 cycle interval centered on the point of interest. The fact that the interval analyzed used data from 200 cycles ahead of the interval center point was incorporated by reporting the indication cycles values as 200 cycles later than the interval center point.

Figures C-3, C-7, C-11, C-15, C-19, C-23, C-27, and C-31 show the smoothed slope of HSE vs the number of cycles plotted with the LCL and UCL calculated point by point as the data progress. These figures show that excursions in average slope above the UCL or below the LCL are one predictor of impending fatigue failure. Furthermore, these excursions above the UCL or below the LCL give considerably greater advance warning of impending failure than can be inferred from the HSE curve.

7. PHASE III EXPERIMENTS

7.1 OBJECTIVE

A series of experiments was designed to record tensile load and tensile strain on two materials and in a number of different specimen and loading types. The test matrix included:

- aircraft aluminum (2024-T3) and construction steel (ASTM A-36);
- uncorroded and corroded condition;
- unnotched condition, containing a central hole (MSD), or containing a notch;
- constant amplitude sinusoidal fatigue loading, stair-step amplitude loading, and stair-step loading preceded by a transient pulse loading; and
- tension, compression, flexure, Mode II shear, and torsion (Mode III notched).

The HSE being consumed by each sample during each fatigue cycle is calculated for each fatigue cycle, and then the nonlinear methods of Sect. 3 are applied for prediction of approaching fatigue failure.

7.2 METHOD

The sample material for the tension-tension aluminum coupon is an unclad 2024-T3 aluminum alloy sheet 0.090-in. thick, a material commonly used in aircraft skins. The coupons were machined to an ASTM E466 standard fatigue specimen with cross-sectional dimensions of 0.5-in.-wide by 1.22-in.-long gage section for the 1-in. extensometer used. To simulate a proof of principle MSD situation, a single No. 15 drilled hole (0.180-in.-diam) was drilled in the center of each specimen's gage section.

Aluminum flexure and Mode II shear specimens of 6061-T6511 aluminum bar 2-in. high × 0.75-in. wide × 15-in. long were prepared. For Mode I flexure testing, a central 1.0- in.-deep notch was added at the center of the specimen, and the specimen was tested with 0.75-in. width and 1-in. ligament depth on a four-point bend test fixture with a 12-in. outer span and a 2-in. inner span in flexure-flexure with R = 0.1. For Mode II

U.S. Patent #5,743,860, April 28, 1998.

shear testing, the aluminum bar was machined into the Mode II notched shear test specimen. However, time and financial restraints did not allow testing of these specimens.

ASTM A-36 construction steel was used for the tests involving low-carbon steel. These were tapered cylindrical tensile coupons and were tested in various modes. Unnotched cylinders were tested in tension-tension, while cylindrical coupons containing lateral 0.25-in. diam holes were tested in tension-tension and in compression-compression. Notched cylindrical coupons containing an external 0.165-in.-deep notch were tested in tension-tension and in torsion-torsion.

In addition, one survey experiment on 2024-T3 aluminum coupons tested in tension-tension was planned at a series of test frequencies from 10 to 0.1 Hz and with R-ratios of 0.1, 0.5, 0.707, and 0.866. However, the available funds did not allow us to conduct this experiment.

Two data variables were recorded from each experiment—tensile load and tensile strain in the reduced section as measured by an extensometer. Loading was performed on a servohydraulic test machine of 25,000-lb tensile capacity at room temperature. The fatigue loading frequency was 0.1 Hz. Data were recorded by a National Instruments PCI 16XE-50 General Purpose I/O System of 16-bit resolution. The data recording frequency was approximately 2000/channel/s, producing ~200 measurements of each variable over each fatigue cycle. Load cell voltage variations were of the order of 0.1% (10 mV) of full scale (10 V), or 10 lb. Measurement resolution was 1 lb in load measurement (~10 psi) and 5 με in strain measurement.

7.3 TEST RESULTS

The first test conducted in this portion of the program was an aluminum tension-tension coupon containing a larger than previously tested central 0.180-in.-diam hole (to simulate a MSD situation at an aircraft rivet hole). The test coupon had been artificially corroded to simulate corrosion encountered in aircraft environmental exposure. The nominal test stress used was 37,044 psi (gross section).

The input strain energy and the HSE exhibited by this specimen as an indicator of future failure was monitored and is shown in Figs. D-1 thru D-4 in Appendix D. The observed response showed a gradual increase in HSE until a level of 0.09 in.-lb/in.^{3} was reached, followed by a sharp falloff in HSE significantly prior to failure. Failure occurred at this stress level after only 1,008 cycles. Nevertheless, a significant forewarning was observed with a corroded specimen in the presence of a hole.

The next specimen tested was a similar tension-tension 2024-T3 aluminum coupon, this time uncorroded, with a central 0.18 in. long × 0.010 in. tall horizontal notch made by electric discharge machining and at constant stress of 38,519 psi. The Input Strain Energy (ISE) and HSE results are shown in Figs. D-5 thru D-8 in Appendix D.

The HSE reaches a plateau of 0.2 in.-lb/in.^{3} for the early part of the fatigue life and begins to rise significantly at about 70% of the fatigue life with the sharpest rise during the final 10% of fatigue life. Thus, specimens which contain simulated small cracks provide easy early recognition of the approach of final failure through this method.

The next specimen tested was another aluminum tension-tension specimen, corroded but unnotched, tested at constant stress of 52,000 psi (compare to specimens TM-1 to TM-7). The results for this specimen are shown in Appendix D, Figs. D-9 thru D-12, and in Table 6.

Table 6. Comparison of uncorroded and corroded aluminum tension-tension specimens

	Specimen							
	Corroded	**TM-1**	**TM-2**	**TM-3**	**TM-4**	**TM-5**	**TM-6**	**TM-7**
Indication based on:	Slope	Curv.	Slope	Slope	Slope	Slope	Slope	Curv.
Cycles for indication >UCL or <LCL	48,690	32,595	41,217	24,985	43,393	43,949	38,997	33,026
Cycles to failure	50,546	33,133	41,955	25,404	43,750	44,727	39,969	34,682
Cycles of life remaining after indication	1,856	538	738	419	357	578	972	1,656
Fatigue life remaining after indication, %	3.67	1.62	1.76	1.65	0.82	1.29	2.43	4.78
Position of failure surface relative to extensometer midspan, 0% = midspan, 100% = span edge	—	175%	175%	0%	100%	100%	150%	125%
Sense of initial HSE change	Falls	Falls	Falls	Falls	Falls	Falls	Rises	Rises

Thus, the method used here for detecting the onset of fatigue failure in 2024-T3 aluminum is as effective, if not more effective, when the aluminum is in the corroded state than when it is uncorroded.

Following this test, a test involving stair-step fatigue amplitude was performed. An uncorroded, unnotched aluminum sample was subjected to a series of fatigue cycle stages of 5000 cycles each, with the fatigue amplitude varying in equal logarithm of stress amplitude intervals between 8,000 psi and 52,000 psi. The ISE and HSE results of this test are shown in Figs. 25 and 26.

The next test involved a tension-tension Mode 1 crack growth test of a tapered ASTM A-36 steel cylindrical coupon which had been artificially corroded and which contained an external 0.165-in.-deep circumferential notch. The specimen was tested with a maximum load amplitude of 42,222 lb and a minimum load amplitude of 4,222 lb at a loading frequency of approximately 0.1 Hz until failure occurred at 3850 cycles. The ISE and HSE results are shown in Figs. D-13 thru D-16 in Appendix D.

The next test conducted was on an A-36 steel tapered cylindrical coupon with a 0.25-in. lateral hole tested in compression-compression. The stress levels used were 38,190 psi, 45,828 psi, and 50,920 psi. The steel was uncorroded, and the stress level was constant amplitude with R = 0.1. The experiment was an attempt

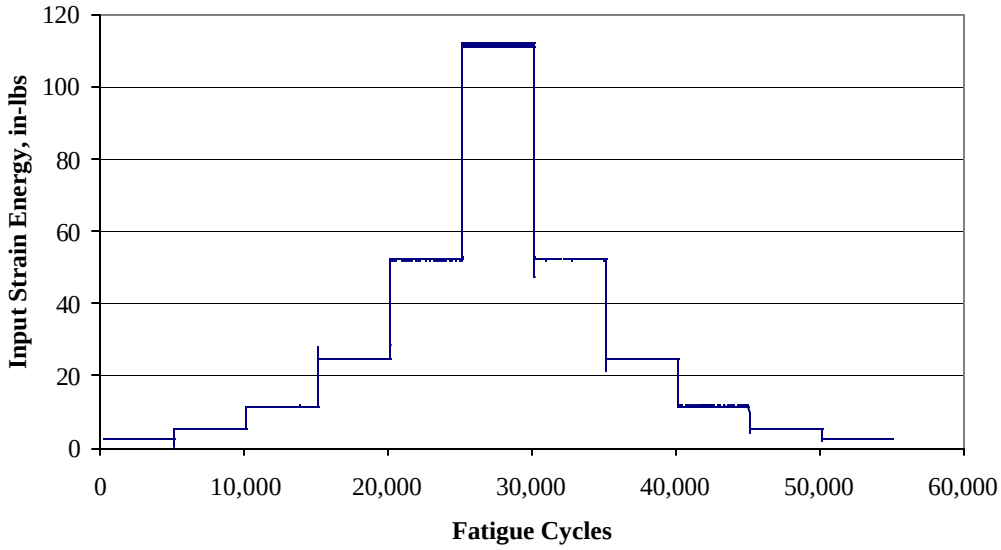

Fig. 25. ISE vs number of fatigue cycles, unnotched uncorroded 2024-T3 aluminum sample SM-TN-AL-UC-SS-UC-1.

to obtain failure by shear under compressive loading, but failure did not occur during the time allotted. The ISE and HSE results obtained are shown in the Figs. D-16 thru D-20 in Appendix D.

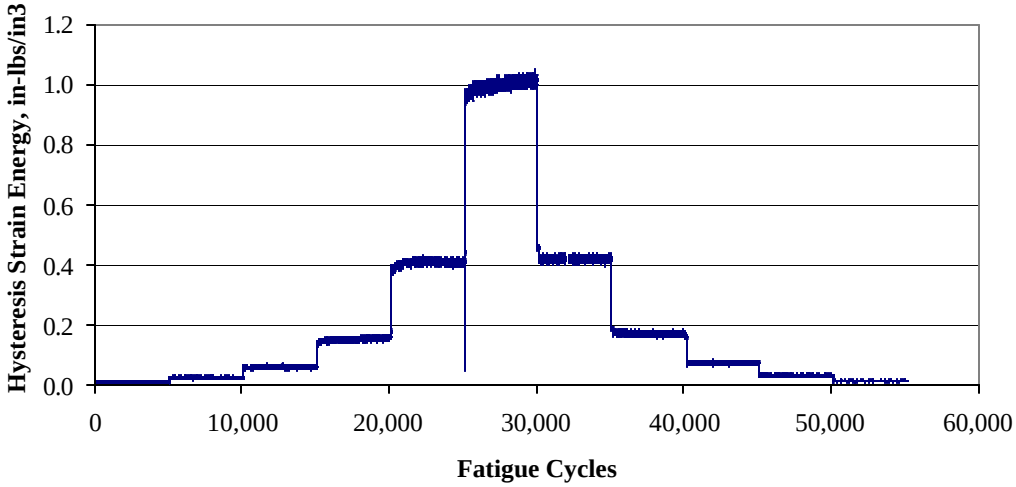

Fig. 26. HSE vs number of fatigue cycles, unnotched uncorroded 2024-T3 aluminum sample SM-TN-AL-UC-SS-UC-1.

Next, an uncorroded A-36 steel tapered cylindrical coupon (Sample SM-TO-ST-UN-CS-NO-1) with an external 0.165-in.-deep notch tested in torsion-torsion or Mode III crack growth. The torsion level used was 187.5 to 1875 in.-lb f torque, and cycling was conducted at approximately 1 Hz. Failure occurred after 27,317 cycles with essentially no forewarning from HSE indications (see Figs. D-21 thru D-24 in Appendix D). This was the first case where no such forewarning was observed. Indications from Knott,[2] p. 117–119, are that Mode III failures in this type of situation are typically unstable with the onset of crack initiation coinciding with final crack propagation, so that, with no subcritical crack propagation or energy absorption mechanism, there would also not be any forewarning of the type proposed here. This may be different for other Mode III test geometries, depending on the form of the material resistance curve, or "R-curve," a plot of crack extension, ? a, vs applied stress intensity factor, K. This curve rises to the point where crack extension initiates, called K_c. If, after that, it continues to rise more slowly, then the material is tough and forewarning can be expected by the presence of subcritical crack growth. If this curve is flat or falls, the material/structure is unstable in that the occurrence of any initial crack growth leads to final failure.

The next test conducted was a simulated low-temperature creep and stress corrosion test using uncorroded, notched 2024-T3 aluminum coupons. A coupon was loaded in tension to a nominal stress-intensity factor of 20.2 ksi%in. (nominal stress of 36,900 psi, 0.3-in. notch) and held at that load for 1.063 h. The load was then increased to 38,750 nominal stress and held at that load until failure at a total time of 169.383 h. The static load and the extensometer displacement were measured vs time. The initial input energy was calculated, and the changes to this integral over time were calculated as a function of time under load. The changes to stored strain energy vs time under load, called HSE for convenience, and the slope of this quantity are shown in Figs. 27–28. Figure 27 shows the energy changes on a logarithmic time scale, emphasizing the initial linear rate of change of energy vs log (time), characteristic of creep processes.

Figure 28, emphasizing the linear rate of change of energy with time, is characteristic of stress-corrosion rate processes. Note, also, the cyclic nature of the energy changes. Each peak and valley represents the interval represented by the addition of a new drop of saline solution in the crack tip, followed by dissipation of this solution, followed by the addition of a new drop. The final rise in value in Fig. 28 is believed to be reliable indicators of stress-corrosion failure, as failure occurred immediately after these indicators.

Following this test, another similar creep/stress corrosion test was conducted on a corroded notched 2024-T3 aluminum specimen. The specimen was held at a constant nominal stress of 42,000 psi and failure occurred after 63.45 min. The HSE results for this sample are shown in Figs. 29–33. Here again, the initial period of approximately 100 s represents logarithmic vs linear crack growth, typical of low-temperature creep crack growth. This is followed by a period where another mechanism seems to become more dominant, probably stress corrosion (see Fig. 29). Note the peaks and valleys in the strain energy slope and curvature during this period, representing the periodic addition of additional saline solution, and the significant fall-off in slope near the end of life.

Finally, we conducted several tests on actual aircraft hardware to determine if the method could be useful in actual operation situations. Our first test article was a section of 7075-T6 aluminum stringer section from stringer 8L of a Boeing 747 aircraft which had flown for 29 years and was currently in the Aer Lingus fleet.

---

[2]J. F. Knott, *Fundamentals of Fracture Mechanics*, Butterworths Publishing, London, 1973.

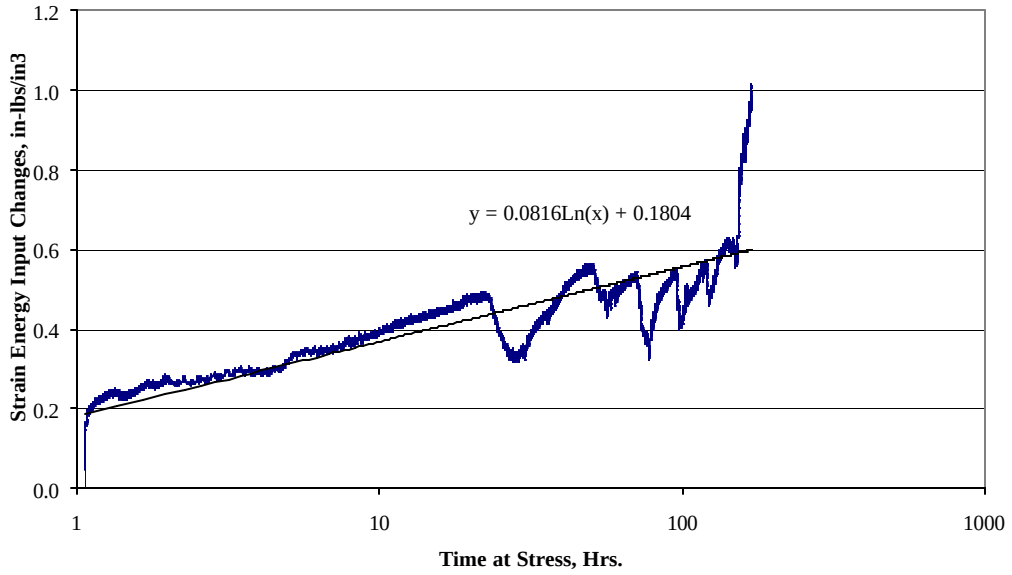

Fig. 27. ISE change vs logarithmic time (low-temperature creep), notched uncorroded 2024-T3 aluminum sample with central 0.180-in. notch at 38,750 psi, sample SM-CR-AL-UC-CS-NO-2A.

A er mainte crews remov section, imately long, near forwar pressu bulkhe the after ng the holes detect during nance.

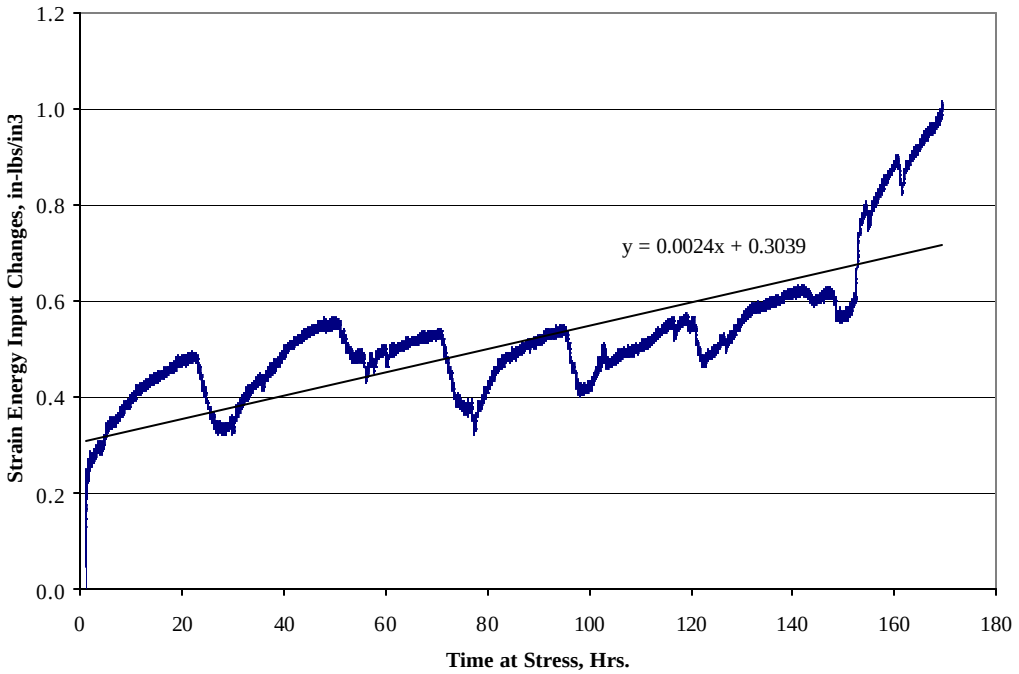

Lingus nance h a d ed the approx 18 in. f r o m t h e d r e ad of aircraft cracki around stringer w a s e d mainte

Fig. 28. ISE change vs linear time (stress corrosion), notched uncorroded 2024-T3 aluminum sample with central 0.180-in. notch at 38,750 psi, with periodic injection of 3.5% saline into notch, sample SM-CR-AL-UC-CS-NO-2A.

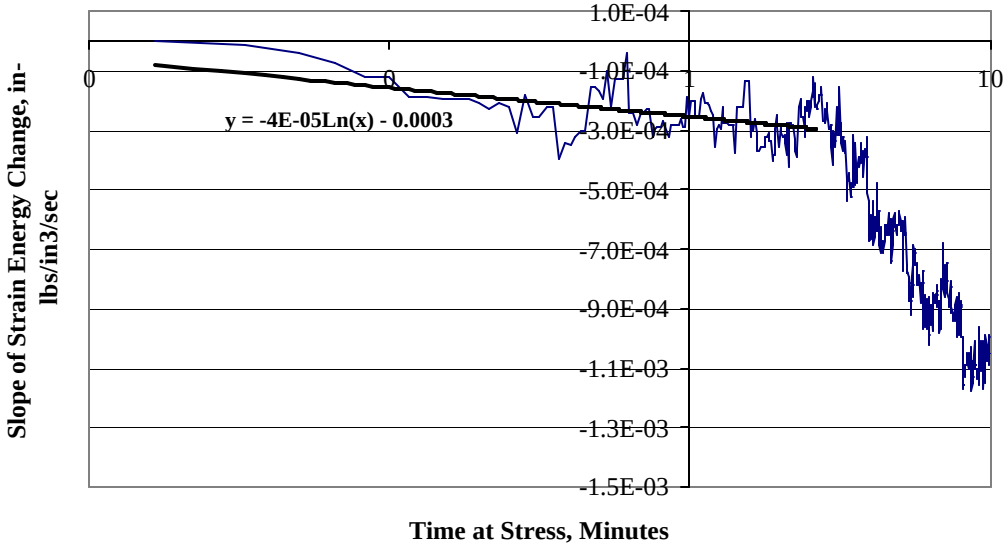

Fig. 29. ISE change vs logarithmic time (low-temperature creep), notched corroded 2024-T3 aluminum sample with central 0.180-in. notch at 42,000 psi, sample SM-CR-AL-CO-CS-NO-1.

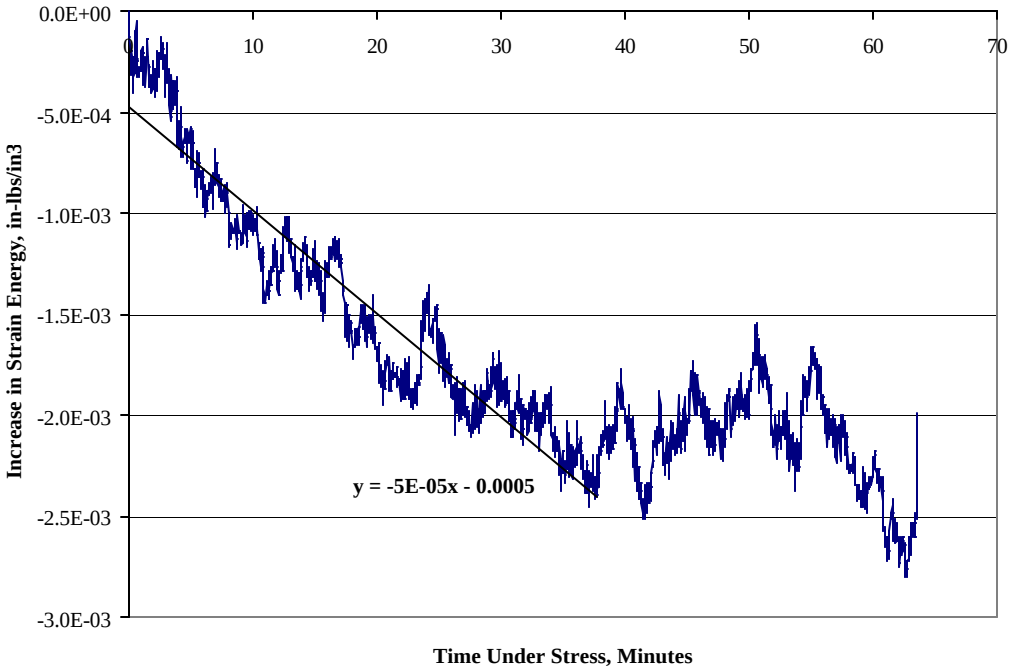

Fig. 30. ISE change vs linear time (stress corrosion), notched corroded 2024-T3 aluminum sample with central 0.180-in. notch at 42,000 psi, sample SM-CR-AL-CO-CS-NO-1.

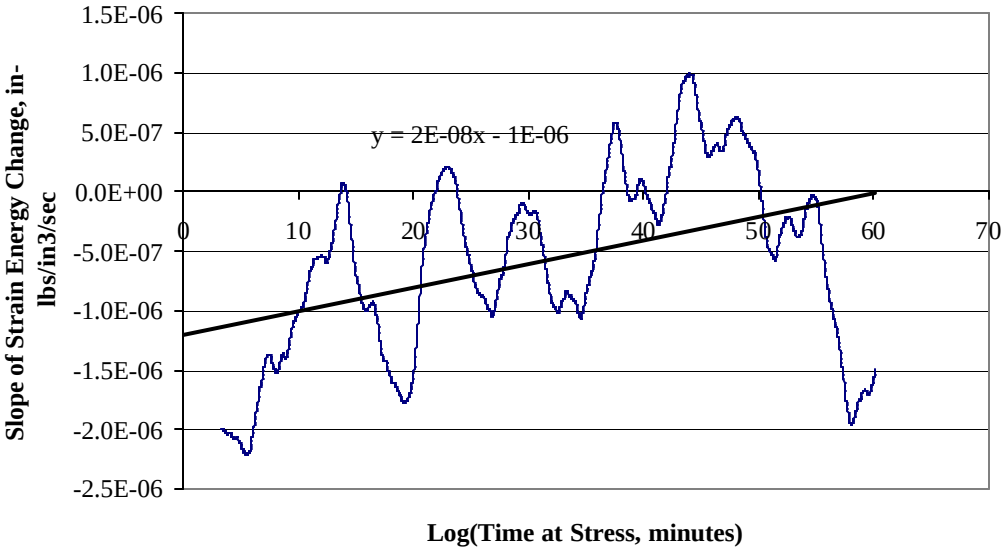

Fig. 31. Slope of ISE change vs linear time (stress corrosion), notched corroded 2024-T3 aluminum sample with central 0.180-in. notch at 42,000 psi, sample SM-CR-AL-CO-CS-NO-1.

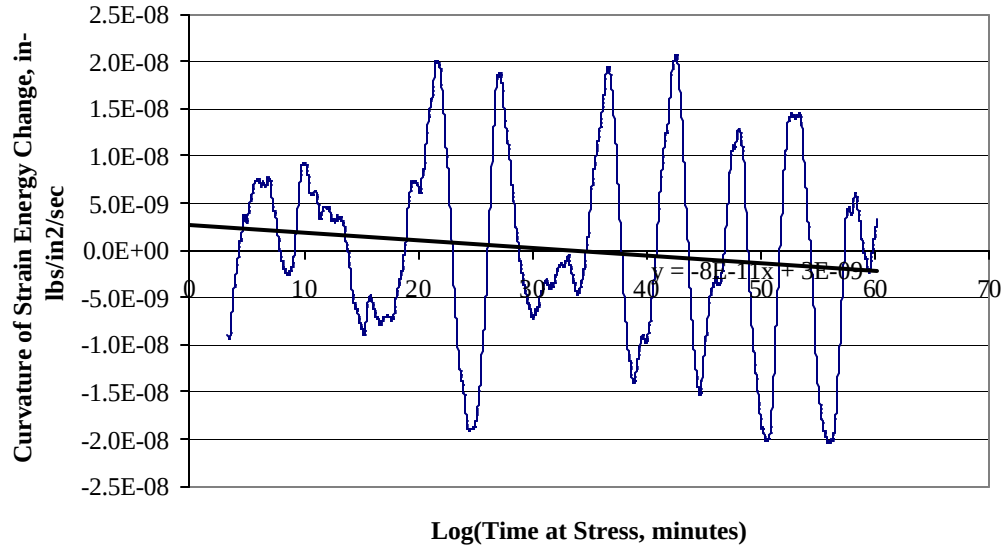

Fig. 32. Curvature of ISE change vs linear time (stress corrosion), notched corroded 2024-T3 aluminum sample with central 0.180-in. notch at 42,000 psi, sample SM-CR-AL-CO-CS-NO-1.

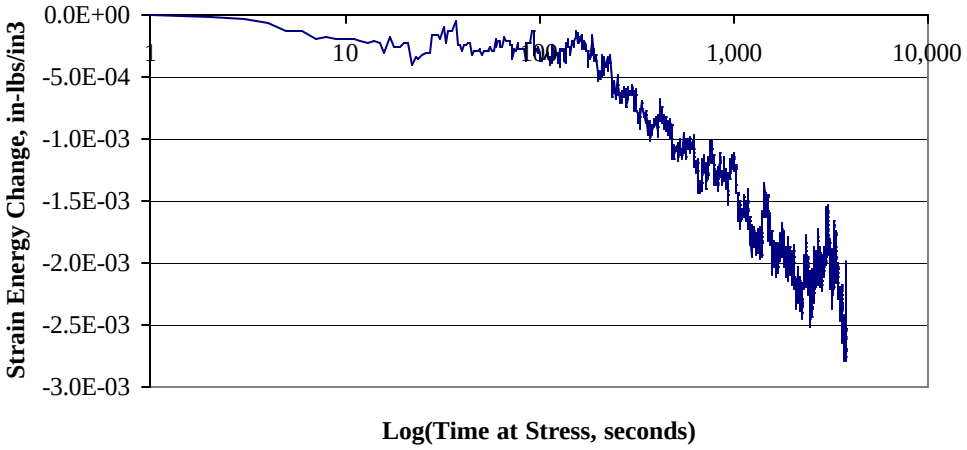

Fig. 33. ISE change vs logarithmic time (low-temperature creep), notched corroded 2024-T3 aluminum sample with central 0.180-in. notch at 42,000 psi, sample SM-CR-AL-CO-CS-NO-1.

The section was cut into a single 15-in.-long piece with a center hole which contained a transverse crack emanating from one side of the hole. In attempting to determine a test load to perform fatigue testing on this cracked piece, the crack extended on the opposite side of the hole, causing failure of the section. It was then decided to cut the remaining stringer section into two 7 1/2-in. sections and to fatigue each section based on the failure moment observed from the original piece.

The first piece of the stringer section tested was fatigued in a four-point bend test fixture with another span of 7 in. and inner span of 2 1/2 in. The reason for testing in a four-point rather than a three-point bend test was to attempt to spread the maximum bending stress field over as many of the far side stringer holes as possible. Load amplitudes of 1845 lb maximum to 184.5 minimum were applied, and failure occurred after 8,387 cycles. The test arrangement, test fixture, and specimen failure are shown in Figs. 34–37. A fatigue crack emanating from the outer edge of one of the far side stringer holes was clearly visible.

The data recorded from this experiment was total bending load and bending fixture inner span displacement. Several problems were initially experienced due to shifting of the test piece so as to creep off of the test fixture. After approximately ten start–stop cycles, this was corrected by adding side guards to the bend test fixture. The resulting ISE and HSE data are shown in Figs. 34–37.

As may be seen from Fig. 38, the sample deformed plastically to a significant extent during its first and subsequent cycles. This plastic deformation represents an energy consumption mechanism, which tends to mask the energy consumption represented by crack initiation and growth. Thus, in the presence of large-scale

plastic deformation of a structure, the nonlinear crack growth monitoring method would not be expected to be a suitable tool for monitoring crack growth.

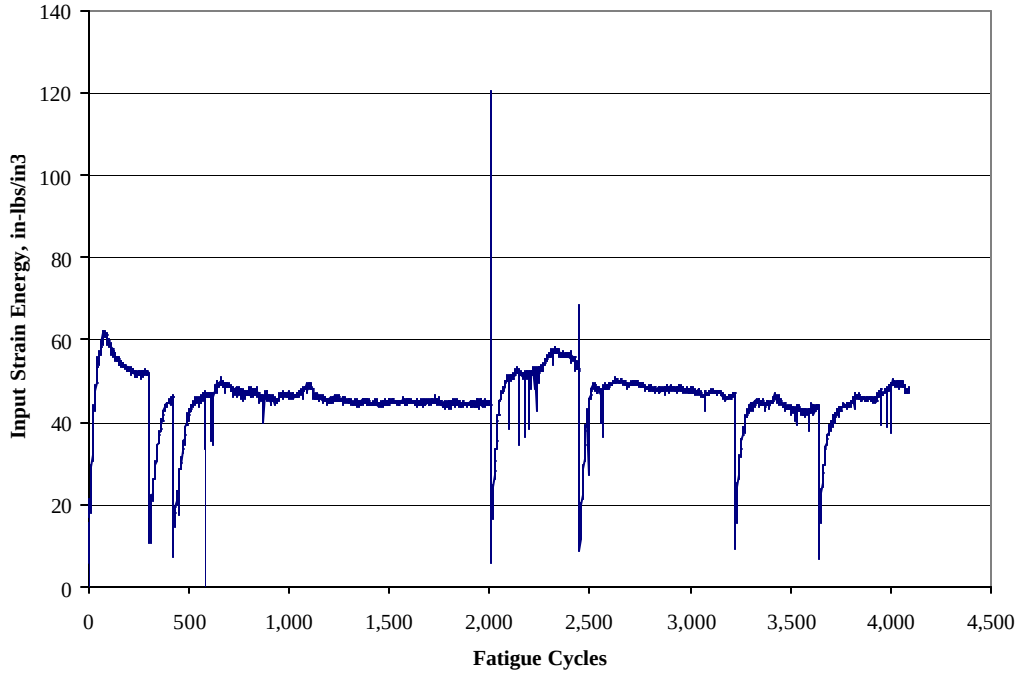

Fig. 34. ISE vs cycles, Aer Lingus stringer section 8L-1, 7075-T6 aluminum.

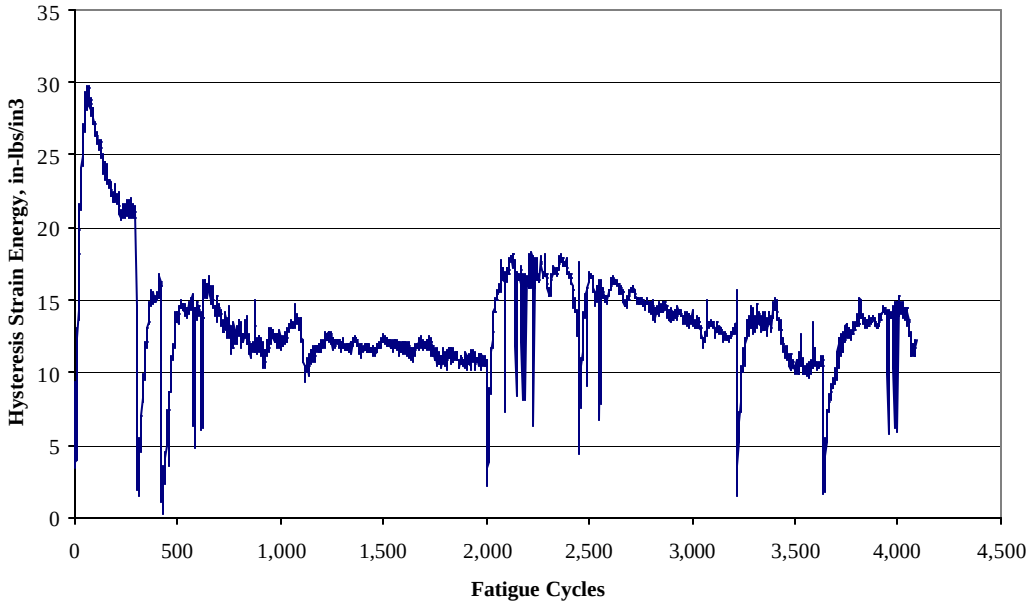

Fig. 35. HSE vs cycles, Aer Lingus stringer section 8L-1, 7075-T6 aluminum.

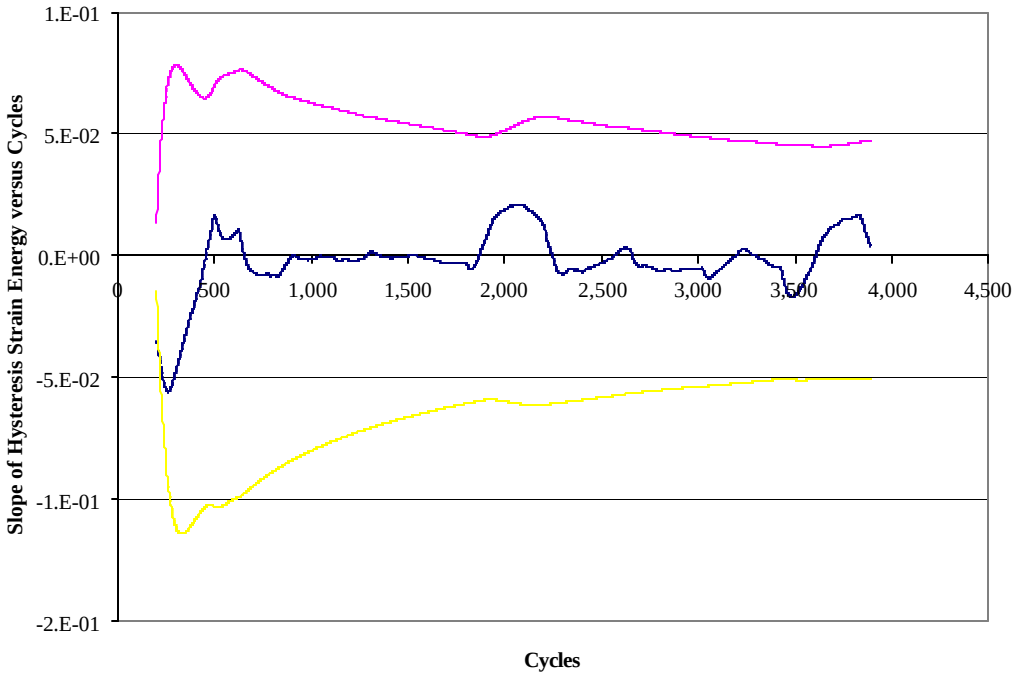

Fig. 36. Slope of HSE vs cycles with UCL and LCL, Aer Lingus stringer section 8L-1, 7075-T6 aluminum.

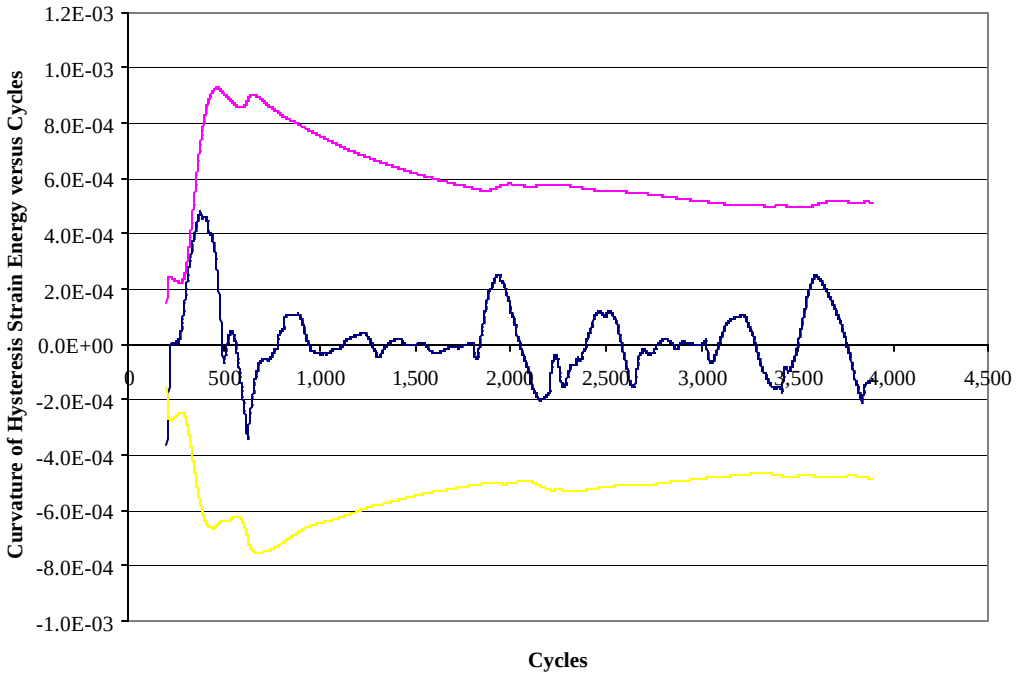

Fig. 37. Curvature of HSE vs cycles with UCL and LCL, Aer Lingus stringer section 8L-1, 7075-T6 aluminum

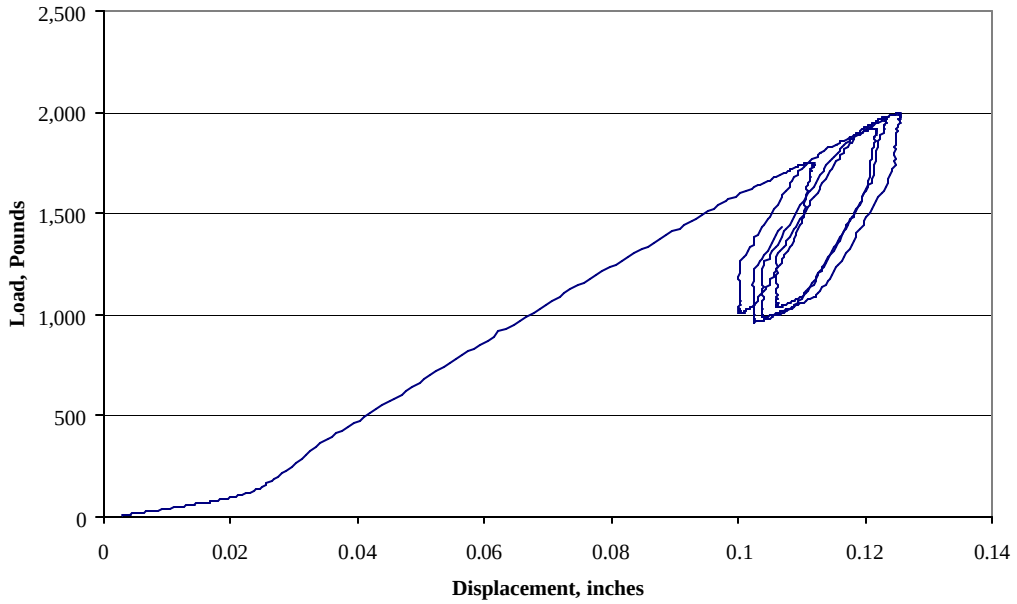

Fig. 38. Load vs displacement for four-point bend test of Aer Lingus Boeing 747 stringer 8L section.

8. OVERALL ANALYSIS AND CONCLUSIONS

8.1 CONCLUSIONS ON HYSTERESIS OR TIME-DEPENDENT STRAIN ENERGY MONITORING

Overall, the results of the experiments shown here provide convincing evidence of the ability to detect the approach of the final stages of crack dominated failure in structures, as demonstrated by monitoring HSE in Mode I, II, or III fatigue, or by monitoring time-dependent changes in strain energy in Mode I, II, or III creep crack growth, or stress corrosion assisted crack growth in metal structures.

In fatigue, using results from Dieter,[1] the constant level of energy absorption, seen in all materials tested, results from many mechanisms which, at higher stresses, collectively go under the name "damping." This damping arises from lack of thermoelastic equilibrium during fatigue, by heating the sample on loading, then undergoing expansion, then cooling the sample during unloading, then contraction of the sample. This damping capacity is said by Dieter to not be very dependent on frequency of vibration but more dependent on stress or strain amplitude and varies significantly from material to material.

---

[1]George E. Dieter, *Mechanical Metallurgy*, McGraw-Hill Book Company, Second Edition, 1976.

Figure 39 shows a ln–ln plot of the level of constant damping energy during fatigue of the fiberglass composite samples vs the applied stress range amplitude.

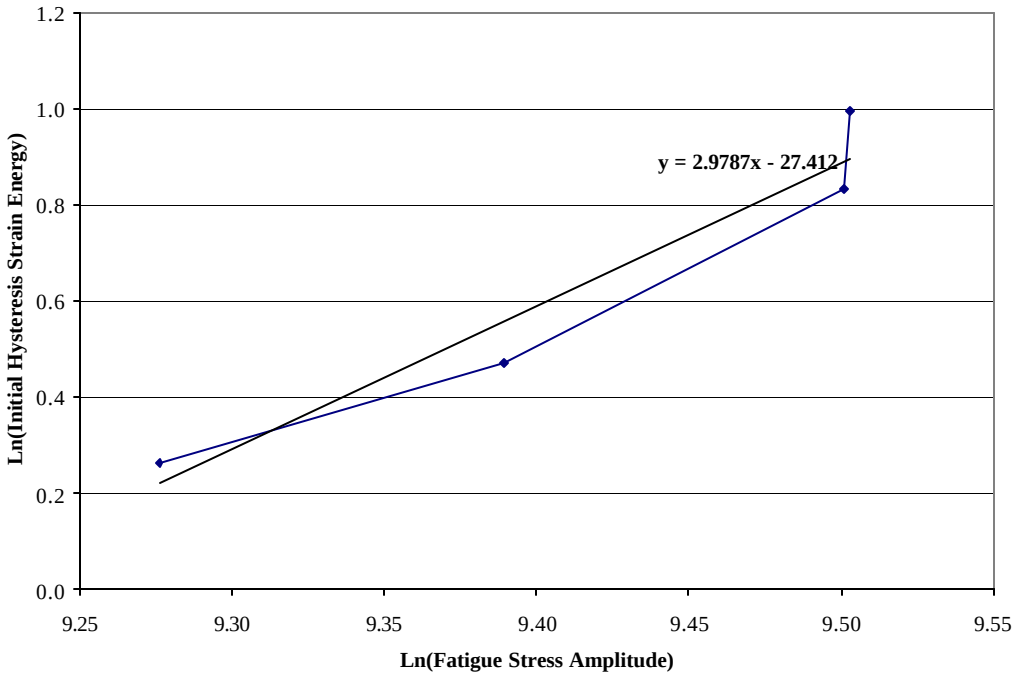

Fig. 39. Log initial HSE amplitude vs log fatigue stress amplitude, initial fiberglass composite samples P36-O-45 thru 48.

As may be seen from the results of tests of various materialsand test geometries at various stress levels (Figs. 39–42), the composite samples exhibited a slightly nonlinear rising HSE vs fatigue stress amplitude with an average HSE vs stress amplitude dependence of HSE ~$S^{2.98}$. For the unnotched Phase I 2024-T3 aluminum samples, the ln–ln dependence of HSE on fatigue stress amplitude was very linear over a broad stress range, with an average HSE vs stress amplitude dependence of HSE ~$S^{2.087}$. For the Phase II aluminum MSD samples with central holes, the ln–ln relationship is somewhat nonlinear but with a downward curvature and the average HSE vs stress amplitude dependence of HSE ~$S^{4.13}$. For the Phase III aircraft aluminum unnotched sample tested in staircase stress amplitude, the results show a ln–ln dependence of HSE vs $S^{2.30}$.

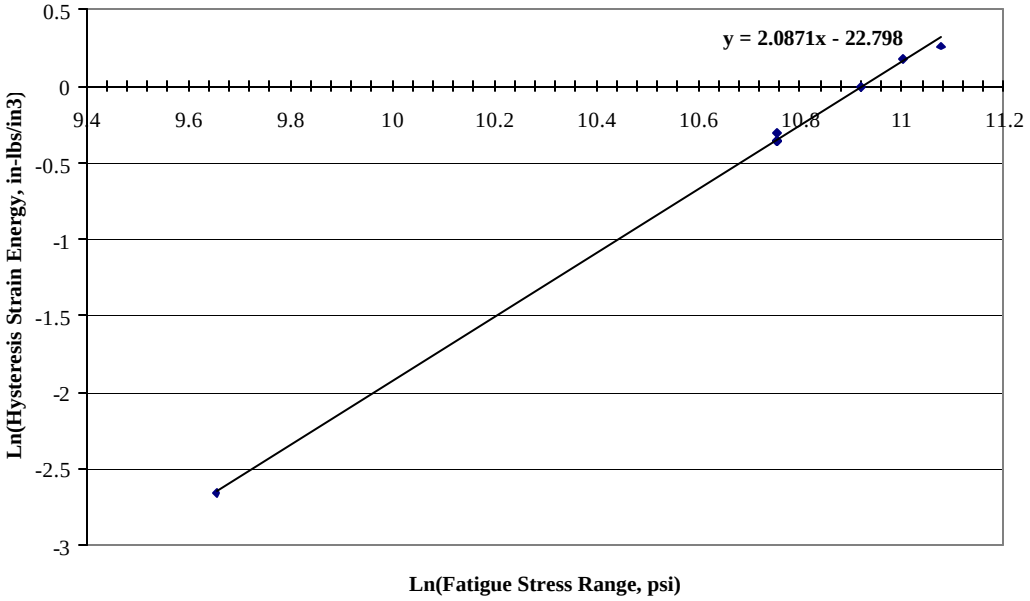

Fig. 40. Log initial HSE amplitude vs log fatigue stress amplitude, Phase I 2024-T3 aluminum unnotched, uncorroded sample, TM-1 thru TM-10.

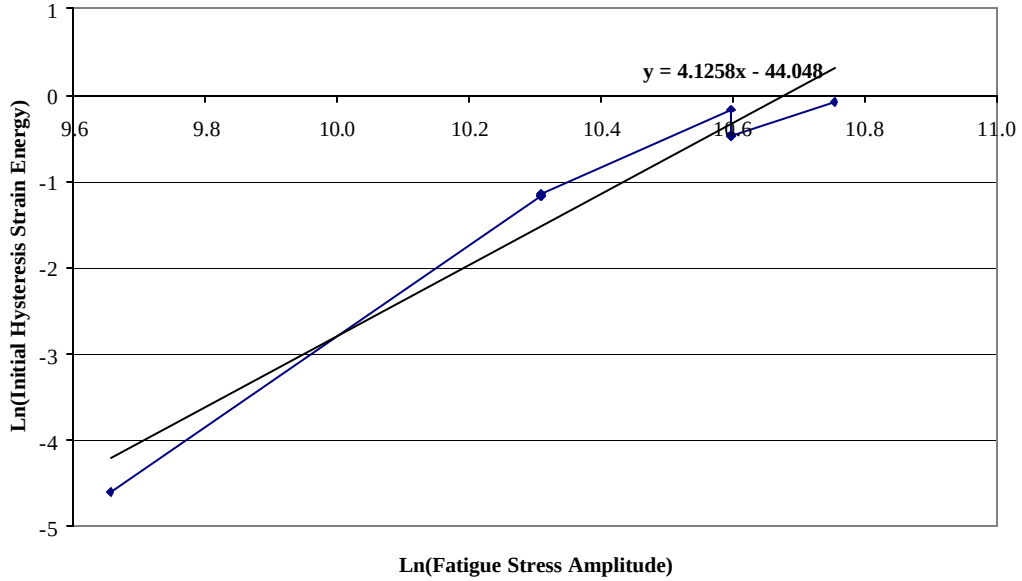

Fig. 41. Log initial HSE amplitude vs log fatigue stress amplitude, Phase II 2024-T3 aluminum unnotched, uncorroded sample, TM2-1 thru TM2-8.

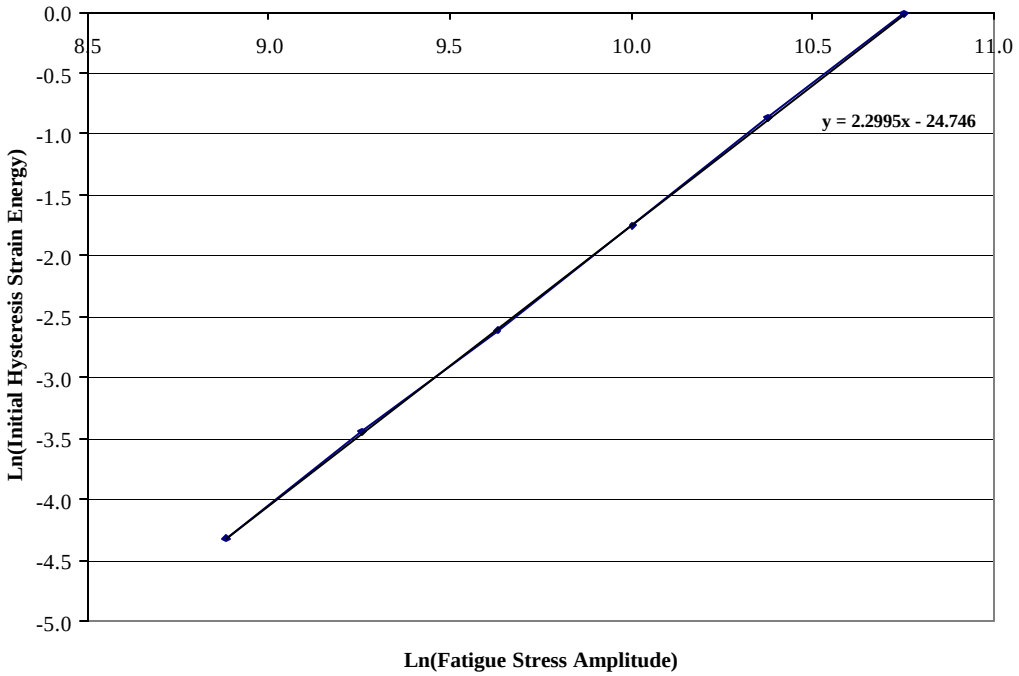

Fig. 42. Ln (initial HSE) vs Ln (fatigue stress amplitude), Phase III aircraft aluminum unnotched staircase loading sample SM-TN-AL-UC-SS-UN-1.

The upward curvature of the composite samples is attributed to the phenomenon of an increasing damage parameter adding to thermoelastic damping of the polymeric material. The downward curvature of the aluminum MSD samples is attributed to the spreading plasticity at the edge of the circular hole and expanding across the uncracked ligament with increasing stress amplitude.

The linear dependence on the initial HSE value, and its value of approximately 2 for unnotched metals, is consistent with the dependence described in Dieter for damping dependence on fatigue stress amplitude.

The important point which these figures show is that each type of structure (basic unnotched material, material containing a hole, material containing a notch) has associated with it a constant and repeatable level of HSE, which may be monitored for sudden increase or decrease as an indicator of the approach of second or third stage fatigue crack growth indicating the approach of fatigue failure.

A typical fatigue crack growth curve for metals is shown in Fig. 43.

From linear elastic fracture mechanics, the Griffith energy for crack extension is numerically equal to

$$G = \frac{K^2}{E} = \frac{dU}{da}, \tag{7}$$

where G is the strain energy release rate, K is the stress intensity factor, E is Young's modulus, U is the potential energy (strain energy) available for crack extension, and da is the incremental crack extension. This quantity, G_c, called the critical strain energy release rate, represents the change in strain energy occurring per unit crack extension.

However, during fatigue, dU is the change in strain energy per cycle. Assuming that this change in strain energy contributes to fatigue crack growth, then this represents the HSE per cycle.

From the fatigue crack growth rate curve, if the ordinate value, da/dN, is multiplied by this constant critical strain energy release rate for the material, dU/da, then

$$\frac{da}{dN} \times \frac{dU}{da} = \frac{dU}{dN}. \tag{8}$$

This means that the quantity of HSE consumed per cycle is linearly related to the quantity of crack growth rate per cycle and, when plotted, produces a curve that is similar in shape to the fatigue crack growth rate curve (see Fig. 43).

During fatigue, crack growth typically occurs in three distinct phases, viz. nucleation, stable crack growth, and unstable final crack growth. During the nucleation phase, the rate of crack growth and, hence, the rate of hysteresis energy consumption is very low and is not apparent above the level of damping energy consumption unless the fatigue stress amplitude is very low. As secondary stage crack growth starts, the rate of energy consumption due to crack growth will, at some point, become significant compared to the level of damping energy consumption so that the total energy consumption being monitored (the HSE) will begin to rise with each cycle. As the final stages of crack growth start, the rise in total HSE consumption per cycle will rise dramatically indicating the imminent approach of final fracture.

Similar mechanisms occur during creep crack growth. However, in creep crack growth, there is no damping energy to mask the internal energy consumption due to creep crack growth. The trilinear form of the creep crack curve [in stress amplitude vs log(time)], similar to the trilinear form of the fatigue crack growth rate curve, will be fully visible by monitoring the rate of energy consumption vs time (see Fig. 29).

Finally, for stress corrosion cracking, a similar trilinear crack growth rate curve will be visible. However, the curve in this case will be of stress amplitude vs linear time elapsed under corrosive environment (see Fig. 30).

Key to all of these techniques is the presence of stable subcritical crack growth preceding final fracture. In the case of the torsional Mode III cracked specimen (see Sample SM-TO-ST-UC-CS-NO-1), the geometry and loading of the specimen seems to have prohibited the occurrence of stable subcritical fatigue growth so that no HSE detection was possible. This behavior in Mode III crack extension is mentioned in Knott.[2]

---

[2]J. F. Knott, *Fundamentals of Fracture Mechanics*, Butterworths Publishing, London, pp. 117–119, 1973.

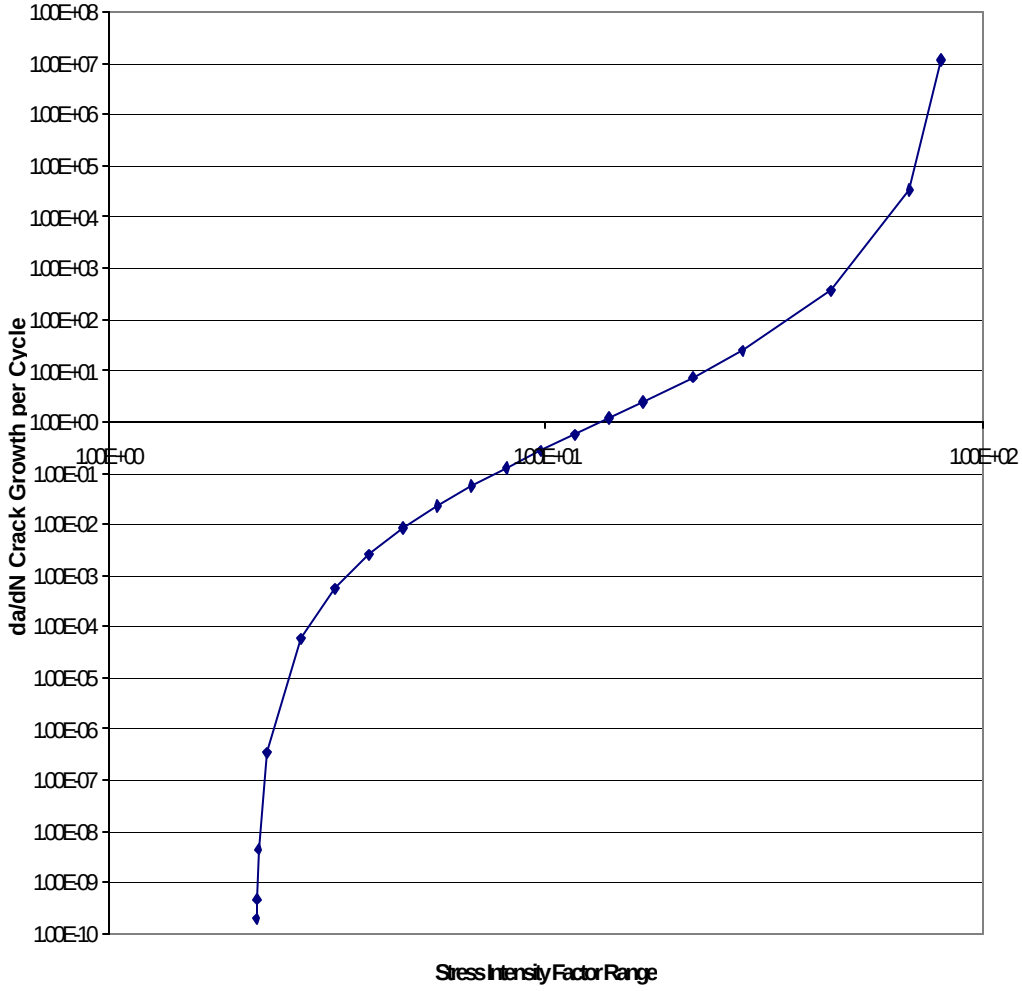

Fig. 43. Typical fatigue crack growth rate curve for metals.

INTERNAL DISTRIBUTION

1. J. R. Corum
2. J. M. Hansen
3. L. M. Hively
4. R. F. Holdaway
5. G. T. Mays
6. D. G. O'Connor
7. M. B. Ruggles
8. T. P. Sjoreen
9. D. E. Welch
10. ORNL Laboratory Records-RC